Struc Bond (2005) 118: 1–57
DOI 10.1007/b137239

Published online: 23 September 2005

Electrochemistry and Electrogenerated Chemiluminescence of Semiconductor Nanocrystals in Solutions and in Films

Allen J. Bard[1] (✉) · Zhifeng Ding[2] · Noseung Myung[3]

[1]Department of Chemistry and Biochemistry, The University of Texas at Austin, Austin, Texas 78712, USA
ajbard@mail.utexas.edu

[2]Department of Chemistry, The University of Western Ontario, London, Ontario N6A 5B7, Canada
zfding@uwo.ca

[3]Department of Applied Chemistry, Konkuk University, Chungju Campus, Chungju, Chungbuk, 380-701, Canada
myung@kku.ac.kr

Abstract A retrospective overview of electrochemical studies of semiconductor nanocrystals (NCs) is given. The electrochemical behavior of monodisperse NCs in a non-aqueous supporting electrolyte can be derived from the electron quasiparticle energy and the electron self-energy. Coulomb blockade can sometimes be observed in Si NCs if the charged NCs are stable. Many NCs, such as Ge, CdS, CdSe, PbS and core-shell CdSe/ZnS undergo some electrochemical and chemical reactions such as the so-called EC reaction mechanism. Electrogenerated chemiluminescence (ECL) processes for elemental and II/VI compound NCs in solution (and their films) are found to follow the general ECL mechanisms of organic compounds. Most NCs emit ECL, which is red-shifted into the photoluminescence (PL) region. ECL studies of NC solid-state films, especially the combination of organic light-emitting diodes (LEDs) and NCs, have suggested the potential for real workable devices. Treated CdSe NC thin films also exhibit stable and fast electrochromic changes and ECL.

Keywords Electrochemistry · Electrogenerated chemiluminescence · Electrochromic response · Semiconductor nanocrystals · Nanocrystal films

1 Introduction

Electrochemical methods of characterizing semiconductor nanocrystals (NCs) can often complement the optical (spectroscopic, microscopic) methods that are usually employed. While absorption and fluorescence spectroscopies mainly probe the interior of the particle and provide information about the electronic transitions (band gap) of the material, electrochemistry mainly probes the particle surface (Fig. 1), as shown in the sections that follow. As with smaller molecules, the electrochemical potentials found for reduction and oxidation provide data on the molecular orbital (MO) energies (Fig. 2) and these can correlate with the band gap of the NC. Moreover, the general voltammetric behavior can show stepwise addition (or removal) of charge, and they yield the diffusion coefficient, D, and information about the stability of the particle upon electron transfer. In addition, as discussed below, one can sometimes see the stepwise charging of the NCs dispersed in solvents as a function of the applied potential.

This chapter deals with the electrochemical characterization of both solutions and thin films of NCs and the electrogenerated chemiluminescence (ECL) in such systems. There are other ways in which electrochemistry impinges on semiconductor NCs. For example, there have been numerous reports of electrochemical synthesis of semiconductor thin films [1] and studies of the photoelectrochemistry (PEC) of NC films [2] (especially films of dye-sensitized nanocrystalline TiO_2 and other semiconductors). These topics will

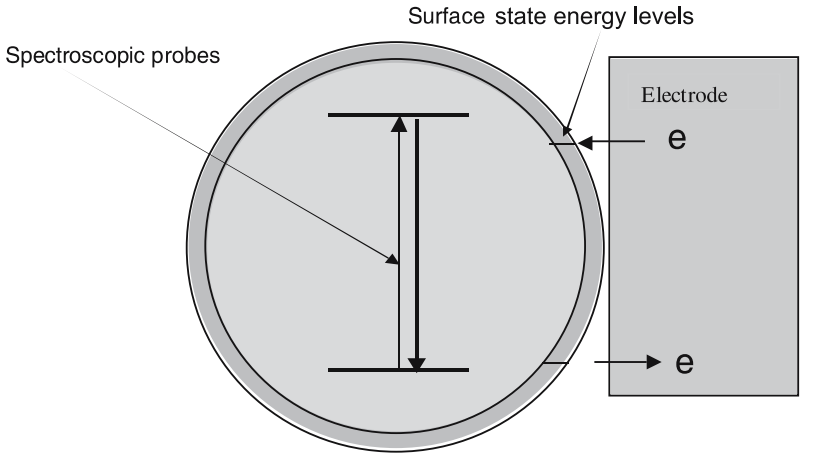

Fig. 1 Schematic representation of light absorption and emission and electrochemical electron transfer processes at a semiconductor nanoparticle

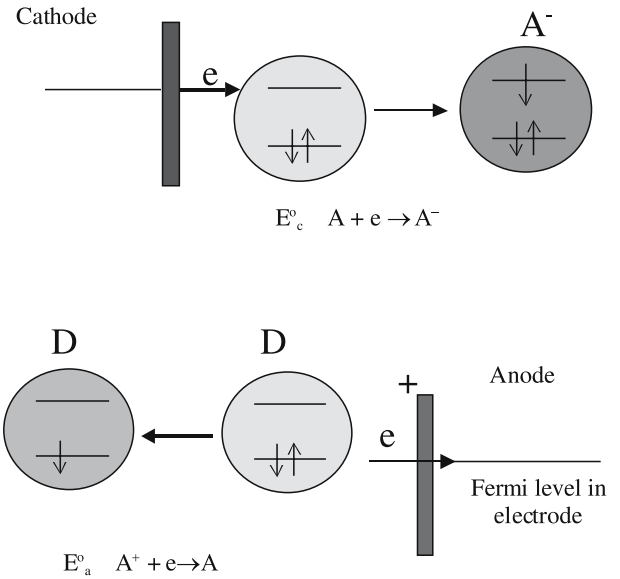

Fig. 2 Schematic representation of electrochemical reduction and oxidation of a NC

not be discussed in this chapter. There have been a number of studies on the electrochemistry of slurries and colloidal dispersions of semiconductors; the next section is a brief overview of this work. The remainder of the chapter deals with more recent studies, especially those that delineate the NC characteristics.

1.1 Early Studies of Dispersions of Semiconductor Nanocrystals

Semiconductor NCs, such as TiO_2 and CdS, were first of interest in connection with photoelectrochemical processes, such as when driving redox reactions at the NC surface by irradiation [3]. Electrochemical studies of semiconductor NCs aimed at studying energy levels in the NCs by noting when the NCs would undergo an electron transfer reaction with an electrode directly or with a species in solution that could then be detected at an electrode under irradiation and in the dark [4, 5].

For example, in a study of TiO_2 NCs in 0.02 M HCl with a collection of photogenerated electrons at an electrode, the action spectrum (collection current vs. wavelength of irradiation) and the photocurrent-potential response could be obtained [5, 6]. These measurements allowed one to obtain information about the NC band gap and the energy levels of electrons and holes in the particles under irradiation. In an alternative approach, reducible species, such as Cu^{2+}, Fe^{3+}, or methylviologen (MV^{2+}) were added to the NC dispersions in order to trap the photogenerated electrons more efficiently [7, 8]. By studying the effect of pH, which shifted the flat band potential (electronic energy level) of the TiO_2 NC with respect to the solution species (MV^{2+}), whose redox potential was pH-independent, the flat band potential could be located at – 0.05 V vs. NHE at pH = 0. Similar experiments were carried out with CdS particles [9, 10] and FeS_2 [11].

Early experiments of this type with colloids of TiO_2 ($\sim$ 2.5 nm) and CdS ($\sim$ 8 nm) in the dark and under illumination at a rotating disk electrode (RDE) demonstrated that these particles showed the expected electrochemical behavior, such as mass transfer-controlled currents as a function of RDE rotation rate and current–potential curves that followed potential-controlled heterogeneous kinetics [12]. Such colloids (TiO_2, SnO_2) were also examined at the dropping mercury electrode [13]. Drawn-out reduction waves were observed that were attributed to the polydispersity of the samples.

These studies of particle suspensions and colloidal dispersions demonstrated the utility of electrochemical measurements in studying semiconductor particles. However, they were carried out with polydisperse preparations, so the unique molecular and NC nature of the systems could not be probed. Moreover, all of these studies were carried out in aqueous solutions, which limited the available potential window that could be explored, compared to the aprotic solvents used in later studies.

1.2 Early Studies of Semiconductor NC Films

Films of discrete NCs, as opposed to bulk films prepared, for example, by chemical vapor or electrochemical deposition, have also been studied. Films

have the advantage of providing a larger electrochemical signal, since one is dealing with a surface effect rather than being limited to low concentrations of particles in solution. A typical study of CdS involved NCs prepared in AOT inverse micelles and attached to a gold surface via a self-assembled monolayer (SAM) of hexanedithiol [14]. The NCs were reasonably monodisperse and the size was estimated from the absorbance spectra. The dark electrochemistry in 0.5 M Na_2SO_4 showed irreversible reduction waves; only the curve for nominal 4 nm NCs showed well-defined waves (Fig. 3). A similar study was carried out with a monolayer of PbS NCs [15].

There have also been electrochemical studies of thicker films of NCs, such as WO_3 and TiO_2 [2, 16]. For example, colloidal suspensions TiO_2 (particle size ~ 8 nm) were spin coated on ITO substrates in layers ca. 0.4 μm thick, and heated to 400 °C [2]. Repeated coatings and firings produced thicker films, up to 4 μm thick. There is also a recent electrochemistry study on capacitive and reactive properties of porous nanocrystalline TiO_2 electrodes in an aqueous electrolyte [17]. Fundamental characteristics such as charge accumulation, charge transport, and interfacial charge transfer were translated into simple electric equivalents, which allow one to identify and classify the major features of the voltammetric response according to the competition between the different processes during current–potential scan. Similarly, films of WO_3 (NC size 2 to 5 nm) up to 10 μm thick were prepared by drop coating and heating [16]. Such films are of interest in electrochromic devices and in solar cells, but do not show the same effects as monolayers of NCs and are not considered further in this chapter.

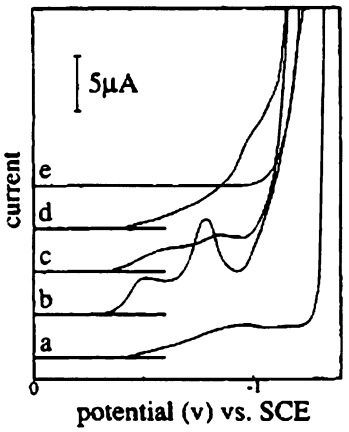

Fig. 3 Dark current-potential curves of **a** CdS (thin film) on ITO; CdS (AOT-capped) NC layers on hexane dithiol SAM with particle size **b** 4 nm, **c** 3 nm, and **d** 2.3 nm. **e** Hexane dithiol SAM [14]

1.3 Electrochemical Reactions in NCs

Several different paths are followed when electrons are injected or removed from a semiconductor NC:

NC charging. For elemental semiconductors, such as Si and Ge, as with Au NCs, addition or removal of electrons can simply lead to charging of the NC (with compensating ions in the solution side of the double layer). Multielectron charging can continue until the field at the particle surface becomes sufficiently high to drive an electrochemical reaction.

NC decomposition. The addition of charge can lead to reduction or oxidation reactions of the NC substituents. For example, for CdS

$$CdS + 2e \rightarrow Cd + S^{2-} \quad \text{(electron injection)}$$

$$CdS - 2e \rightarrow Cd^{2+} + S \quad \text{(hole injection)}$$

NC doping. Charge added to the NC can be compensated for by moving an ion into the NC lattice. For example, the addition of an electron to WO_3 is compensated for by moving H^+ from solution into the semiconductor. This is sometimes called "*n*-doping". Hole injection could be compensated for by an anion, and this would constitute "*p*-doping".

2 Theoretical and Experimental Background

The principles of electrochemistry and electrogenerated chemiluminescence for monodisperse NCs in solutions and NC film will be outlined in this section. The experimental procedures for both methods will be briefly described. Literature was followed to prepare Si [18], Ge [19], CdS [20–22], CdSe [20, 23–25], PbS [26, 27], PbSe [28] as well as CdSe/ZnS core-shell [29] NCs. For the detailed synthesis and size-selective separation methods used to prepare semiconductor NCs, please refer to Peng's chapter in this book and [30].

2.1 Electrochemistry of Monodispersed NCs

Monodispersed semiconductor NCs can be coated with dielectric organic molecules such as trioctylphosphine oxide (TOPO), alkyl thiols and alcohols, and dissolved in an organic electrolyte solution that has a wide potential window. The applied potential is the potential difference between a working electrode where an electrochemical reaction takes place and a reference electrode that has a fixed potential. An electrochemical reaction at the working

electrode is driven by the applied voltage [31, 32]:

$$\mathrm{Ox} + \mathrm{e}^- \Leftrightarrow \mathrm{Red}\,, \tag{1}$$

where Ox is the oxidized state and Red the reduced state.

When the working electrode in a NC solution is changed to a negative potential, electrons can be added to the NCs through the dielectric organic layer (an electrochemical reduction or injection of electrons) (Fig. 2). The charging energy required to add the first electron to a single NC, μ_1, equals the electron quasiparticle energy, ε_{e1}, which depends on the size-dependent shift in the LUMO (energy level $e1$ in Fig. 4), ε^0_{e1}, and the electron "self-energy" $\sum_{e1}$, which results from its image charge due to the dielectric constant discontinuity of the surrounding dielectric media [33]:

$$\mu_1 = \varepsilon_{e1} = \varepsilon^0_{e1} + \sum\nolimits_{e1}\,. \tag{2}$$

ε^0_{e1} describes quantum confinement and $\sum_{e1}$ represents dielectric confinement [33]. Calculated values of $\sum_{e1}$ typically range from 0.2 to 0.5 eV for Si NCs in the size range of interest here [33]. The charging energy required to add the second electron to the LUMO of a negatively-charged NC μ_2 has the component for the extra electron-electron coulomb interaction $J_{e1,e1}$:

$$\mu_2 = \varepsilon^0_{e1} + \sum\nolimits_{e1} + J_{e1,e1} = \varepsilon_{e1} + J_{e1,e1}\,. \tag{3}$$

The addition of the third electron to the energy level $e2$, requires the charging energy:

$$\mu_3 = \varepsilon^0_{e2} + \sum\nolimits_{e2} + 2\,J_{e1,e2} - K_{e1,e2} = \varepsilon_{e2} + 2\,J_{e1,e2} - K_{e1,e2}\,, \tag{4}$$

where $K_{e1,e2}$ is the exchange energy between the parallel spin electrons in the $e1$ and $e2$ energy levels.

The electron "addition energies" are defined as the differences between the charging energies:

$$\Delta^{(e)}_{N+1,N} = \mu_{N+1} - \mu_N\,. \tag{5}$$

The addition energy for the second electron is

$$\Delta^{(e)}_{1,2} = \mu_2 - \mu_1 = J_{e1,e1}\,. \tag{6}$$

Similar expressions can be developed for the addition energies of the holes $\Delta^{(h)}_{N+1,N}$ in the process of electrochemical oxidation of NCs. For instance, the addition energy of the second hole in the HOMO (energy level $h1$) is

$$\Delta^{(h)}_{1,2} = \mu_{-1} - \mu_{-2} = J_{h1,h1}\,. \tag{7}$$

A classical estimation of $J_{e1,e1} \approx e^2/2C_{\mathrm{NC}}$ reveals that the sub-attofarad (aF) capacitances for NCs give rise to $\Delta^{(e)}_{1,2} \gg k_{\mathrm{B}}T$; in other words the addition energy is greater than the thermal fluctuation energy, even at room temperature, leading to discrete charging events in the potential scans [32, 34–36].

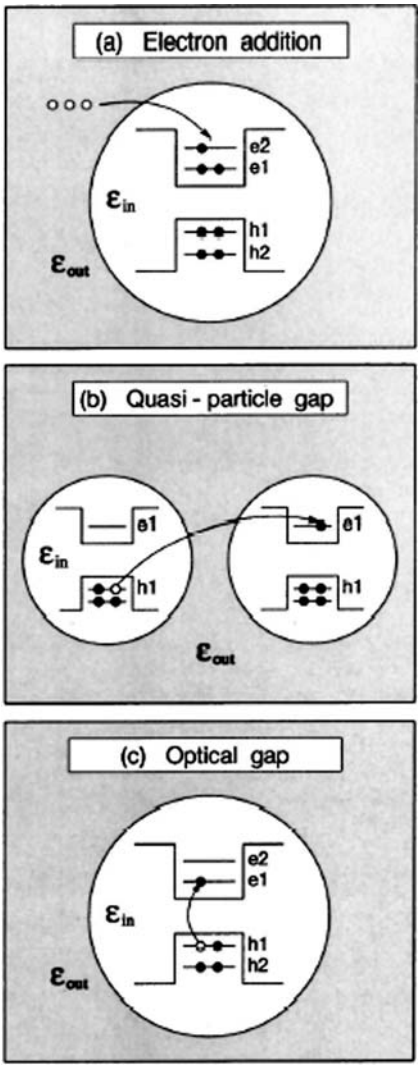

Fig. 4 **a** Illustrates the process of loading three electrons into an otherwise neutral QD. **b** Shows the process of removing a single electron from a QD and placing it into an identical dot at infinite distance. **c** Describes the process of optically exciting an electron-hole pair in a neutral QD [33]

Murray and co-workers [34] introduced the term quantized double layer (QDL) charging for thiol-capped metal clusters to differentiate this collective electrochemical response from coulomb blockade phenomena observed for single-charge injection to isolated individual dots in scanning tunneling spectroscopy (STS) experiments (also called "addition spectra" [37]). Unlike the electrical response measured by STS, the electrochemical current is limited by

quantum dot (QD) diffusion to the electrode surface. The electrochemical behavior is very sensitive to the NC size variation. This is due to the small size of the NCs, where electron addition is quantized [38]. On the other hand, if C_{NC} is independent of the number of electrons injected, consecutive charge injection should occur in regular potential steps, $\Delta V = e/C_{NC}$. For example, organic capped Au NCs [34] show discrete peaks for charge injections. Fifteen evenly spaced (ΔV) peaks characteristic of charge injection to the metal core were recently reported by Quinn et al., because of degenerate metal band structure [39]. Nonetheless, the charging energy, μ_i, required for electron or hole addition is the same for STS and differential pulse voltammetry (DPV) measurements. For example, an electrochemical coulomb staircase was recently observed based on two nanometer-sized electrodes connected in series through a solution containing a redox couple [36]. Furthermore, electrochemistry of semiconductor NCs will reveal richer information than metallic NCs because of their more complicated band structure. Indeed, Banin et al. have identified atom-like electronic states in indium arsenide NC QDs using cryogenic STS [40]. Finally, the electrochemical intermediates might not be stable. Mechanisms like electrochemical reactions accompanied by chemical reactions (EC mechanism) can be easily distinguished using the electrochemical behavior of the NCs (see for example Sect. 3.2.1 in the case of CdS NCs).

Cyclic voltammetry (CV) is a technique frequently used to measure the current during the process of linearly changing (at a given scan rate) the potential

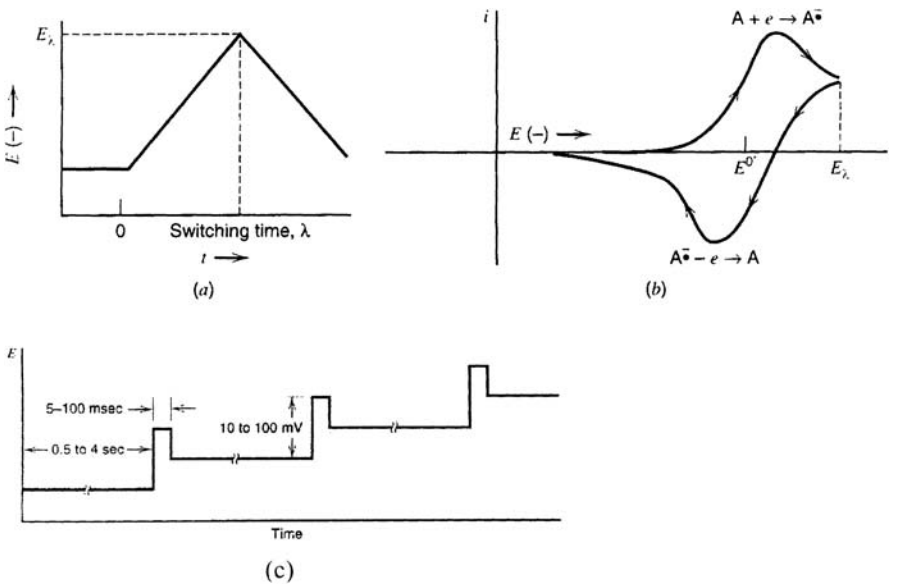

Fig. 5 **a** Cyclic potential sweep. **b** Resulting cyclic voltammogram. **c** Potential profile of DPV [32]

between two limits, E_i and E_f, on the working electrode (Fig. 5a,b) [31, 32]. CV provides a lot of information about electrochemical reaction mechanisms. However, the technique has low sensitivity (minimum concentrations around 10^{-6} M) because of the large background current that arises from capacitive charging of the electric double layer, faradaic reactions of impurities and electrolyte, and oxidation or reduction of the electrode surface [41].

DPV can be used to suppress the background signal and enhance the sensitivity. The potential-time waveform for DPV is shown in Fig. 5c. The differential current is the current at the end of the pulse minus the current observed just prior to the pulse as the applied potential advances from one pulse to the next [31, 32].

2.2 Electrogenerated Chemiluminescence (ECL)

ECL takes place from an excited species that is formed in the course of an electrochemical reaction. We begin with ECL in a solution. In ECL experiments, electron transfer annihilation of electrogenerated anion and cation radicals results in the production of excited states [32, 42]:

$$R^{\bullet -} + R^{\bullet +} \rightarrow R^* + R \tag{8}$$

$$R^* \rightarrow R + h\nu \tag{9}$$

ECL has been extensively studied for organic molecules such as aromatic hydrocarbons and heterocycles, as well as for complexes like $Ru(bpy)_3^{2+}$ [32, 42, 43]. In this chapter, $R^{\bullet -}$ and $R^{+\bullet}$ refer to negatively- and positively-charged NCs electrogenerated at the working electrode, which then react in solution to give the excited state R^*.

An alternative approach to generating ECL is through the use of a coreactant. The purpose of the coreactant in ECL is to overcome either the limited potential window of a solvent or poor radical anion or cation stability [32]. For example, the oxidation of oxalate (the coreactant) produces a strong reducing agent, $CO_2^{-\bullet}$, which can then react with the cation radical $R^{+\bullet}$:

$$C_2O_4^{2-} \rightarrow C_2O_4^{-} + e \tag{10}$$

$$C_2O_4^{-} \rightarrow CO_2^{-\bullet} + CO_2 \tag{11}$$

$$R^{+\bullet} + CO_2^{-\bullet} \rightarrow R^* + CO_2 \tag{12}$$

Similarly, the reduction of peroxydisulfate (as a coreactant) releases a strong oxidizing agent $SO_4^{-\bullet}$, which can interact with an anion radical $R^{-\bullet}$:

$$S_2O_8^{2-} + e \rightarrow S_2O_8^{2-\bullet} \tag{13}$$

$$S_2O_8^{2-\bullet} \rightarrow SO_4^{2-} + SO_4^{2-\bullet} \tag{14}$$

$$R^{-\bullet} + SO_4^{-\bullet} \rightarrow R^* + SO_4^{2-} \tag{15}$$

2.3 Electrochemistry Procedures: CV and DPV

A typical electrochemical cell consists of a Pt disk working electrode (0.06 cm^2), a Pt wire counter electrode, and an Ag wire quasi-reference electrode. A quasi-reference electrode is used to prevent contamination of the aprotic solvent with water and other species; its potential is usually measured with respect to a true reference electrode at the end of the experiments. The Pt working electrode is polished with 0.05 μm alumina slurries (Buehler), and then sonicated in water. The Pt electrode is frequently cycled in 0.1 M H_2SO_4 between – 0.5 and + 0.6 V at 10 V/s (for 400 cycles) to obtain a cleaner and more reproducible Pt surface.

NC solutions typically contain about 5 to 50 mg of NCs with 0.1 M tetra-*n*-butylammonium perchlorate (TBAP) or 0.1 M tetra-*n*-hexylammonium perchlorate (THAP) as a supporting electrolyte in pure *N*,*N*′-dimethylformamide (DMF), acetonitrile or CH_2Cl_2. Solutions are usually prepared and loaded into an airtight cell in a drybox filled with He (Vacuum Atmospheres Corporation, Los Angeles, CA, USA). CVs and DPVs are obtained with a suitable electrochemical workstation, such as Autolab (Eco Chemie, Utrecht, the Netherlands) or a CHI 610A (CH Instruments, Austin, TX, USA). Typical experimental parameters for DPVs are: 0.05 V pulse height, 60 ms pulse width, 200 ms period, 0.02 V/s scan rate.

2.4 ECL Experiments: Voltammetric ECL, Potential Step and ECL Spectrum

CVs and voltammetric ECL curves were obtained simultaneously using an electrochemical workstation coupled to a photomultiplier tube [PMT, for example a R4220p held at – 750 V with a high-voltage power supply series 225 (Bertan High Voltage Corp., Hicksville, NY, USA)]. The ECL signal, measured from the PMT as a photocurrent, was transformed into a voltage signal by an electrometer (such as Model 6517, Keithley, Cleveland, OH, USA). ECL spectra are recorded with a charge coupled device (CCD) camera (such as CH260, Photometrics, Tucson, AZ, USA) cooled below – 110 °C with liquid nitrogen focused on the output of a grating spectrometer (such as Chemspec 100S, American Holographics Inc., Littleton, MA, USA). Spectra are recorded with the working electrode pulsed between fixed potentials; for example at 1 to 10 Hz frequency.

2.5 ECL Experiment of Si NC Film

In this experiment [44], indium-tin oxide (ITO)-covered glass (Delta Technologies, Stillwater, MN, USA) was thoroughly cleaned by sonication, first

in acetone for 15 min, then for 20 min in a 20–30% (v/v) solution of ethanolamine in highly pure Millipore water at 60 °C, followed by several rinsing/sonication steps with pure water at room temperature to remove traces of ethanolamine, and dried under a stream of pure nitrogen. Si NCs were redispersed in acetonitrile that was filtered through 0.2 μm syringe filters before use. NC films (around 100 nm) were spin-coated (Headway Research, Garland, TX, USA) from the acetonitrile solution at 1000–2000 rpm, onto clean ITO-covered glass or other substrate. After spin coating, the film was dried under high vacuum at room temperature for 8 h. Ga : Sn (Alfa-Aesar, Ward Hill, MA, USA) liquid contacts were printed using a syringe. The current–light emission–voltage curves were taken using an AUTOLAB electrochemical station coupled to a Newport (Irvine, CA, USA) optical power meter. Measurements were performed at room temperature. More detailed procedures are given in publications on thin-film solid-state electroluminescent (EL) devices based on tris(2,2′-bipyridine)ruthenium(II) complexes [45, 46].

3
Electrochemistry and ECL of Semiconductor NCs

3.1
Elemental Semiconductor NCs

Elemental semiconductors, such as Si and Ge, have the advantage of being relatively stable on reduction and oxidation (in the absence of water), compared to compound semiconductors (such as CdS) discussed in Sect. 3.2. These, then, allow measurement of quantum charging effects in the absence of currents from decomposition reactions.

On the other hand, there has been interest in NCs of indirect band gap semiconductors such as Si and Ge, especially due to the properties of obtaining useful levels of PL in the visible region of the spectrum and possible applications in optoelectronics and microelectronics [47–51].

3.1.1
Electrochemistry and ECL of Si NCs

The electrochemical properties of freely diffusing Si NCs dispersed in DMF measured at a Pt electrode are shown in Fig. 6 [52]. Discrete steps associated with single electron charging and a large central gap between the onset of oxidation and reduction, characteristic of the energy difference between the highest occupied and lowest unoccupied MOs (the HOMO–LUMO gap) were observed. The observed response was stable on repetitive potential cycling

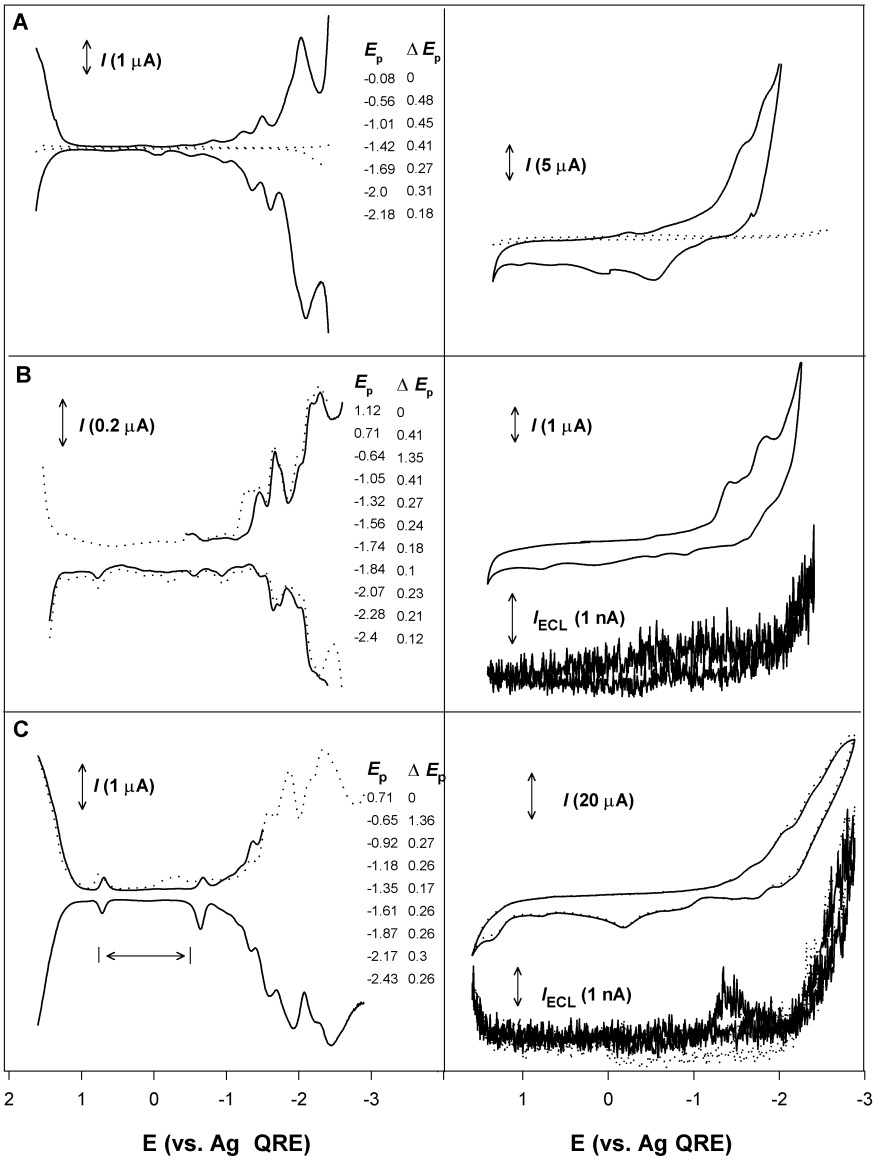

Fig. 6 Cyclic voltammograms (*right panels*) and differential pulse voltammograms (*left panels*) for several batches of Si nanoparticles in 0.1 M tetrahexylammonium perchlorate (THAP) DMF solution. *I*, current; E_p, current peak potential, ΔE_p, potential difference between two succeeding peaks; I_{ECL}, ECL photocurrent from the photomultiplier tube; QRE, quasi-reference electrode. The NCs' size and dispersion were **a** 2.77 ± 0.37, **b** 2.96 ± 0.91, and **c** 1.74 ± 0.67 nm. Cyclic voltammetric ECL voltage curves are plotted in **b** and **c**. The *dotted curves* in **a** represent the response of the blank supporting electrolyte solution. The *dotted curves* in **b** and **c** are the responses for different initial DPV scan potentials [52]

over long time periods with no evidence of fouling or film formation on the Pt electrode surface. Typical electrochemical responses for different solutions of Si NCs are given in Fig. 6, with NC sizes of (a) 2.77 ± 0.37, (b) 2.96 ± 0.91 and (c) 1.74 ± 0.67 nm. For example, in Fig. 6a there are as many as five well-resolved DPV peaks between 0 and – 2.1 V. These almost regularly spaced peaks appear reversible and highly reproducible.

Although the DPV peaks in Fig. 6 were not separated by exactly the same ΔV, the average $\Delta V \approx 0.4$ V corresponds to a capacitance of approximately 0.4 aF/cluster (Fig. 6a):

$$C_{\mathrm{MPC}} = \frac{\mathrm{e}}{\Delta V} \tag{16}$$

This is comparable to the value reported for organic capped noble metal clusters [53]. The ΔV compares favorably with values reported for organic capped Au NCs, and recent calculations by Franceschetti and Zunger for Si QDs with $\Delta_{1,2}^{(e)}$ on the order of 0.4 to 0.6 eV [33]. As discussed in Sect. 2.1, the irregularly spaced electrochemical behavior of NCs depends on both the electron quasiparticle energy and the electron "self-energy", while the electrochemical behavior of metallic NCs is determined only by the electron "self-energy". With increasing NC charge, ΔV decreases measurably, perhaps due to the band structure, multi-electron effects or NC size dispersity, which can smear the observed responses in Fig. 6a,b [53]. The electrochemical behavior seen in these figures was very sensitive to the NC size variation (± 0.37 nm in Fig. 3a and ± 0.91 nm in Fig. 6b).

The DPV responses in Fig. 6a–c are from NCs of different sizes. Common features include the appearance of a large central gap ($(\mu_1 - \mu_{-1} > 1.3$ V); the subscript "– 1" refers to the hole chemical potential) and the general absence of DPV peaks in the positive potential region. This last feature was not a limitation of the available electrochemical window, as seen in Fig. 6a where the DPV response in the absence of Si NCs is given. Electron injection occurred as discrete charging events; however, NC oxidation (hole injection) was not generally quantized and the DPV response was characterized by a continuous increase in current with potential indicative of multiple charge transfers. Nevertheless, the forward and reverse DPV scans are relatively symmetric, indicating that both single and multiple charge transfers are reversible. This contrasts with the electrochemical response of comparable CdS and PbS NCs [26, 54], where electron and hole injection were irreversible and multielectron transfer processes were proposed (the injected charge was consumed by fast coupled chemical reactions due to cluster decomposition). The large size-dependent central gap relates to the energetic difference between the highest occupied and lowest unoccupied MOs (the HOMO–LUMO gap) [34], reflecting the quantized electronic structure of the semiconductor

NC (from Eq. 2):

$$\mu_1 - \mu_{-1} = \varepsilon^0_{e1} - \varepsilon^0_{h1} + \sum\nolimits_{e1} + \sum\nolimits_{h1} . \tag{17}$$

The optical gap $\varepsilon^{\text{opt}}_{\text{gap}}$, on the other hand, relates to ε^0_{e1}, ε^0_{h1}, and the *electron-hole* coulomb interaction $J_{e1,h1}$:

$$\varepsilon^{\text{opt}}_{\text{gap}} = \varepsilon^0_{e1} - \varepsilon^0_{h1} - J_{e1,h1} . \tag{18}$$

Therefore,

$$\left(\mu_1 - \mu_{-1}\right) - \varepsilon^{\text{opt}}_{\text{gap}} = \sum\nolimits_{e1} + \sum\nolimits_{h1} + J_{e1,h1} . \tag{19}$$

The HOMO-LUMO gap increases with decreasing NC size from 2.96 ± 0.91 nm in Fig. 6b to 1.74 ± 0.67 nm in Fig. 6c. However, as will be discussed later, the electrochemical response can be dominated by the particle surface, so this apparent electrochemical gap can be affected by the presence of non-passivated surface states that can act as local traps for electrons and holes. As much as 30 to 50% of the surface of the NC may be ligand-free and coated with a mixture of H, Si – C = O and possibly a small amount of oxide [18]. Thus, the electrochemically-measured gaps are probably not representative of the bulk of the particle (Fig. 1).

Density functional and quantum Monte Carlo calculations on the silicon nanocluster, $Si_{35}H_{34}$ with a diameter of 2 nm and its passivated derivatives with F, Cl, OH, O and S groups revealed a density of states very similar to the electrochemical behavior observed (Fig. 7) [55].

The NCs obtained are efficient emitters of visible light, with quantum yields of between 5% and 20% and size-tunable colors that can range from blue to red [18]. This is rather remarkable, given that the indirect band gap of bulk Si makes it a poor candidate for a light-emitting material. Although the precise origin of the light emission is still unknown [56], quantum confinement in Si has led to efficient PL [57, 58], and radiative transitions have been observed [59] in a variety of Si nanostructures, including thin wires [60], dots [18] or porous silicon [59, 61].

In order for ECL to occur through electron transfer annihilation of electrogenerated charged NCs (reactions 8 and 9), the intermediates must be chemically stable and maintain their charged states long enough to transfer charge upon colliding with oppositely-charged NCs in solution. Si NCs seem to fulfill this requirement according to the observed electrochemical behavior. Light emission by charge injection, ECL, into freely diffusing NCs occurred under repetitive electrode potential cycling (see Fig. 6b,c) or pulsing (Fig. 8) between NC oxidation and reduction. This was the first report of solution ECL from NCs [52]. The relative ECL intensity was greater in the potential region where anionic NCs are electrogenerated (Fig. 6a and c). This may indicate that the electrogenerated oxidized forms are more stable. Light emission was not observed when the applied electrode potential was not suf-

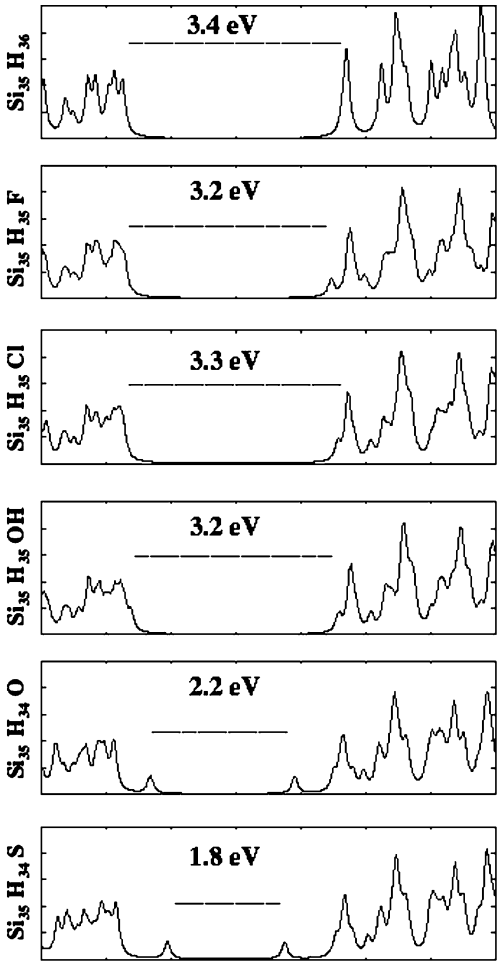

Fig. 7 Local density approximation (LDA) calculated density of states (Lorentzian broadened) of a $Si_{35}H_{36}$ cluster passivated with F, Cl, OH, O, and S groups. The single particle gaps are marked by the *horizontal bar* [55]

ficient to generate both the negatively- and positively-charged species. The ECL spectrum (Fig. 9a) obtained from the annihilation (reaction 8) in MeCN, where the applied electrode potential was pulsed between the oxidation and reduction potentials (double potential step) in 100 ms steps [32, 42], showed a maximum at 640 nm. The coreactant systems (reactions 2 and 15) reveal similar spectra (Fig. 9b,c).

The ECL spectra in the above three cases all show a maximum wavelength of 640 nm, substantially red-shifted from that in the PL spectra (e.g., Fig. 9b). The orange ECL emission was not sensitive to NC size or the capping agent used. On the other hand, the Si NC is size-dependent [18]. A few important

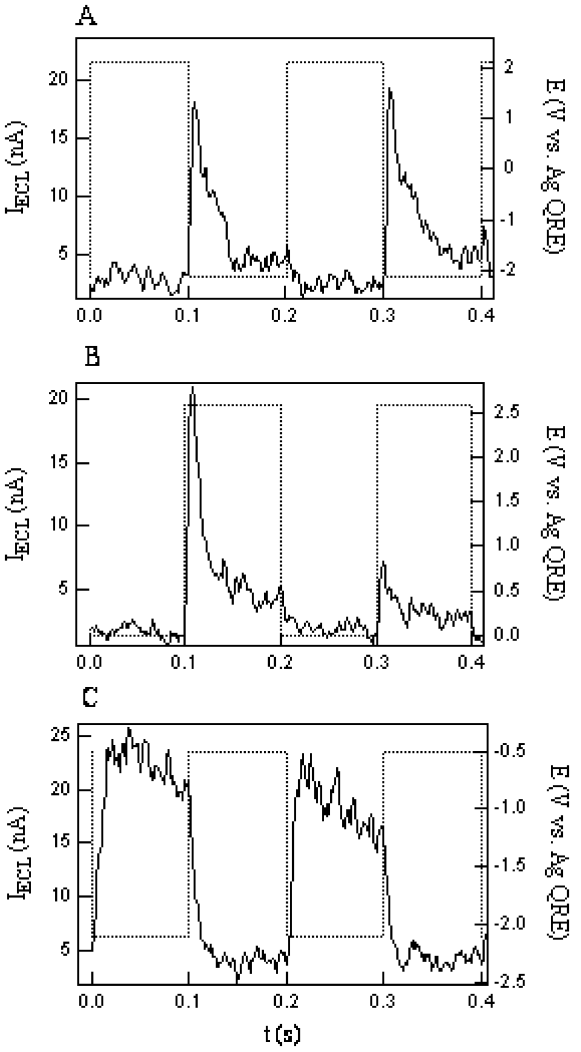

Fig. 8 ECL transients for **a** annihilation of cation and anion radicals in 0.1 M THAP MeCN solution, **b** an oxalate coreactant system with 2.5 mM tetrabutylammonium oxalate added to the solution of **a**, and **c** a peroxydisulfate coreactant system in 0.1 M THAP DMF solution with 6 mM tetrabutylammonium peroxydisulfate added. The nanoparticles are 2 to 4 nm in diameter. *Dotted curves* indicate applied potential steps; *solid curves* indicate ECL transients. *t*, time [52]

observations and conclusions can be drawn from the ECL data. First of all, the electrochemical "turn-on voltage" (the potential gap in Fig. 6b,c) for radiative electron-hole annihilation between positively- and negatively-charged NCs exceeds the optical transition energy. This observation is consistent with the fact that electron and hole injection into separate NCs requires greater en-

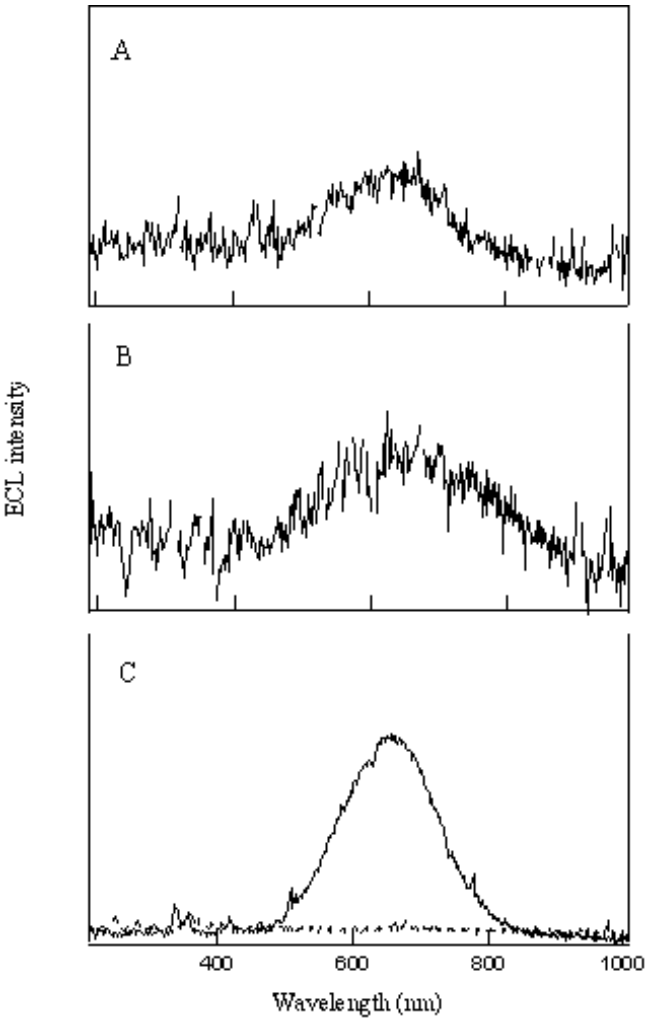

Fig. 9 ECL spectra for **a** annihilation of cation and anion radicals generated by stepping the potential between 2.7 and – 2.1 V at 10 Hz with an integration time of 30 min in the same solution as in Fig. 8a; **b** an oxalate coreactant system, stepping the potential between 0.1 and 3 V at 10 Hz, integration time 40 min in the same solution as in Fig. 8b; and **c** a peroxydisulfate coreactant system, stepping the potential between – 0.5 and – 2.5 V at 10 Hz, integration time 10 min in the same solution as in Fig. 8c. The *dotted curve* in **c** is the ECL spectrum for the blank solution [52]

ergy than optical excitation. Second, the turn-on voltage for ECL significantly exceeds $\mu_1 - \mu_{-1}$. Although the potential difference $\mu_1 - \mu_{-1}$ enables electron and hole injection, and electron transfer between charged NCs in solution is possible, the carrier energies are not large enough to produce bulk *radiative* electron-hole recombination. This observation is consistent with previous

observations for Si NCs. Excitation energies for efficient PL are found to significantly exceed the absorption edge, with a PL intensity that depends sensitively upon excitation energy, as shown in Fig. 10b. Furthermore, the PL energy is considerably greater than the absorption edge, indicating that the lowest-lying energy levels do not result in strongly radiative transitions.

Quantitatively, however, the energetic difference between the PL and ECL of approximately 0.8 eV suggests that the emitting states are different. Previously, for Si NCs passivated with alkoxide-linked hydrocarbon chains [56], the indirect band-gap was reported to shift from the bulk value of 1.1 eV to $\sim$ 2.1 eV for NCs of about 2 nm diameter and the direct transition appeared to blueshift by 0.4 eV from its 3.4 eV bulk value over the same size range. In that case, violet PL ($\sim$ 365 nm) was the most intense emission and was attributed to direct electron-hole recombination, while other, less intense PL peaks ($\sim$ 580 nm) were assigned to surface state and phonon-assisted recombination (Fig. 11) [56]. Undoubtedly, ECL depends more sensitively on surface chemistry and the presence of surface states. PL mainly occurs via excitation and emission *within* the NC core, although the electron and hole wave functions can interact strongly with the NC surface. Despite a few notable exceptions [62, 63], charge injection to a Si NC is generally assumed to occur via its surface states, given the large surface area and the possible presence of many dangling bonds. If we consider the Si NC/oxalate coreactant system (reactions 10–12) as an example, the Si cores have band gaps greater than the energy separation of the surface states, which are only slightly affected by the NC size (Fig. 10a) [64]. As the electrode potential is made more positive, holes are injected into the particle. Concurrently, oxalate is oxidized

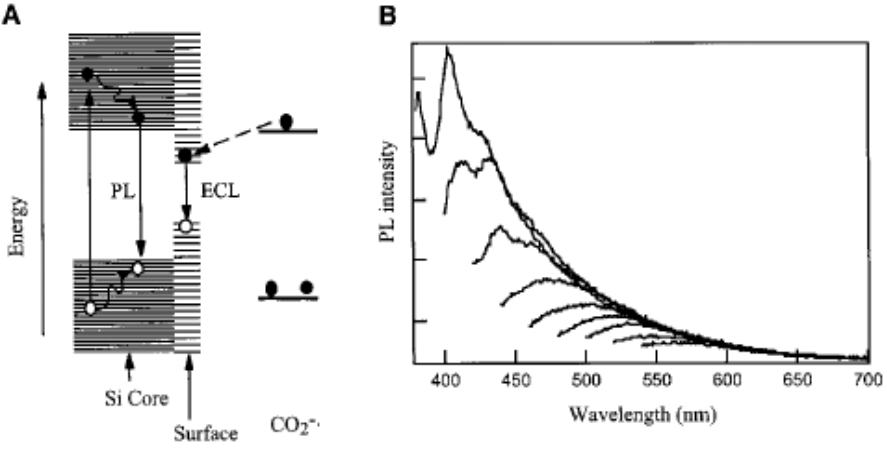

Fig. 10 **a** Schematic mechanisms for ECL and PL of Si clusters. **b** PL spectra at different excitation energies recorded with the same solution as in Fig. 8a. The excitation wavelength from top to bottom was between 360 and 520 nm at 20 nm intervals [52]

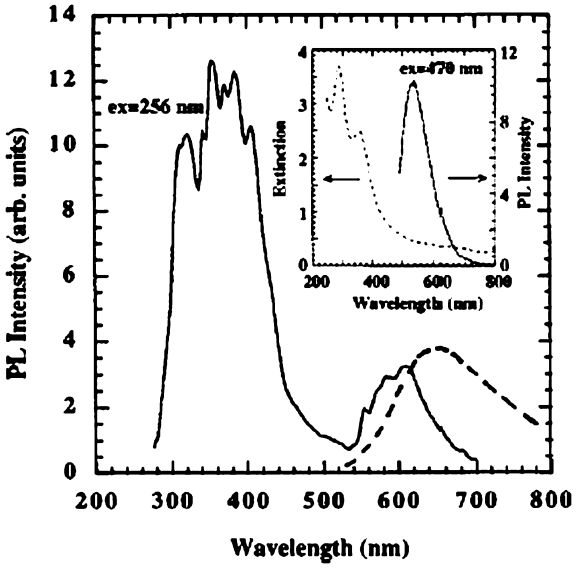

Fig. 11 The PL spectrum of an as-prepared $d < 5$ nm Si NC sample. The *dashed curve* is for $d = 5$ nm Si nanoclusters capped by SiO_2 excited at 350 nm. The *inset* shows a coplot of the extinction and PL spectra for a $d = 4.0$ nm Si NC sample [56]

and then undergoes a chemical reaction generating the powerful reducing agent $CO_2^{-\cdot}$. This intermediate injects an electron across the NC surface (reaction 10) and makes emission possible through surface electron-hole recombination. The other two ECL processes (reactions 8 and 15) are assumed to occur via a similar mechanism. The observed ECL emission insensitivity to core size and capping agent supports this proposed mechanism. Thus, the difference in light emission through PL and ECL from the same Si NCs most likely results from the greater significance of surface states for charge injection as opposed to photoinjection (Fig. 1). Note that similar long wavelength emission is found with porous Si produced by anodic etching in the presence of organic surface modifiers [65]. However, in that case, various Si surface species containing H and O, may also be involved.

In addition, theoretical calculations on Si NCs [55] have demonstrated that quantum confined states represent just one mechanism responsible for the observed optical gap in Si NCs, and that the specific surface chemistry must be taken into account in order to quantitatively explain their optical properties (Fig. 7).

3.1.2 ECL of Ge NCs

Bulk Ge, with a band gap of 0.67 eV, is an interesting material for photonic applications in the IR region. However, there is only one study on the electrochemical properties of Ge NCs [66].

Fig. 12 shows voltammetric ECL light emission from the Ge NCs in a DMF solution containing 0.1 M TBAP. The Ge NCs used were synthesized by the arrested-growth method in supercritical octanol. They were polydisperse in nature, with an average size of 4.5 nm and capped with an organic layer of C8 hydrocarbon chains bound through an alkoxide layer [19]. ECL was observed through an annihilation mechanism when the electrode potential was cycled between + 1.5 V and – 2.3 V at a scan rate of 1.0 V/s. Several important features were observed. First, electrogenerated reduced species are more stable than oxidized ones, as indicated by the relative ECL light intensity. Also, a relatively sharp peak was observed in the potential region where oxidized forms are electrogenerated, implying differences in the generation kinetics of the charged species. On the other hand, the light emission upon reduction is

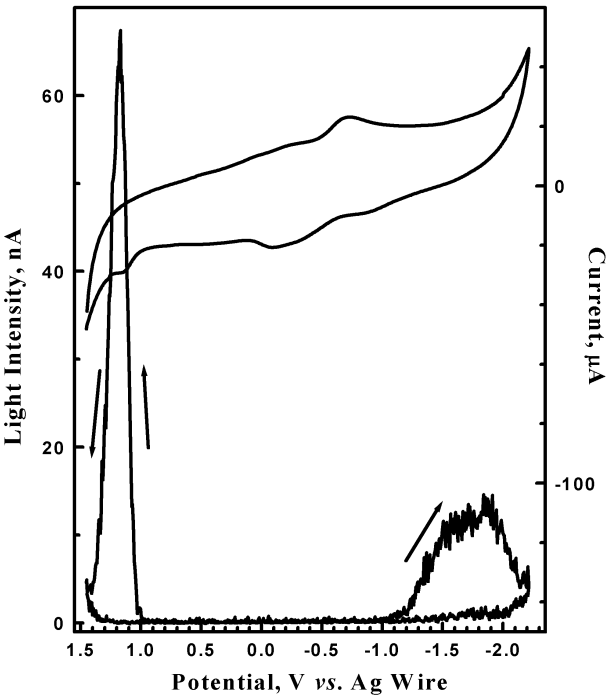

Fig. 12 Cyclic voltammogram and ECL curve of Ge NCs in DMF containing 0.1 M TBAP (scan rate: 1.0 V/s) [66]

lower and broader in intensity. Poor electrochemical behavior was observed with the CV and DPV, which is similar to the case of CdSe NCs [67] described below, because the NC concentration is limited by their solubility to the μM range.

ECL transients for annihilation of oxidized and reduced forms were obtained by switching the electrode potential between oxidation and reduction of Ge NCs. As seen in Fig. 13, an initial step from 0.0 V to – 2.5 V generated weak and broad ECL light. Similar behavior, a so-called preannihilation process, was observed and discussed in a publication [67]. The next step to 1.5 V generated substantially sharp and intense light emission through the annihilation mechanism. ECL light intensity was higher when the potential was stepped to the oxidation potential, suggesting again that reduced forms of Ge NC are more stable. However, ECL light generated upon oxidation decayed faster than the light generated upon reduction, as seen in Fig. 12, and this may be related to the broad peak in Fig. 13.

Fig. 14 shows the ECL spectrum obtained from the Ge NCs dispersed in a DMF solution containing 0.1 M TBAP using a double potential step between + 1.5 V and – 2.5 V at 10 Hz for 30 min. The ECL spectrum shows a maximum

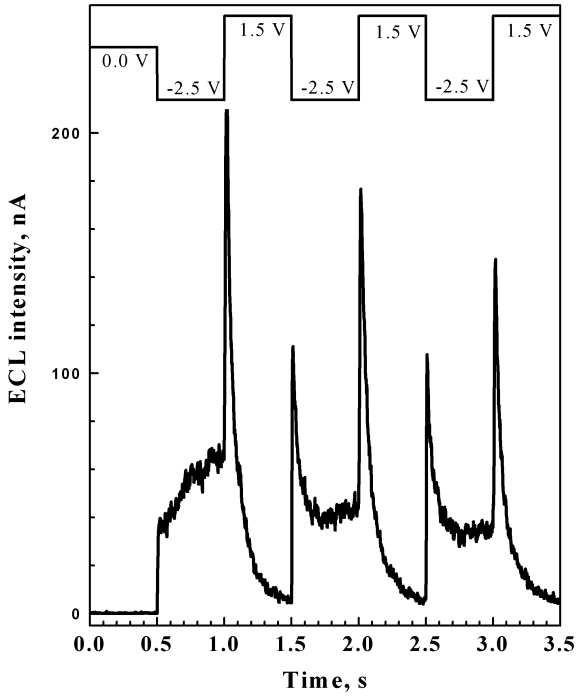

Fig. 13 ECL transients of Ge NCs in DMF containing 0.1 M TBAP obtained by the potential steps between + 1.5 V and – 2.5 V [66]

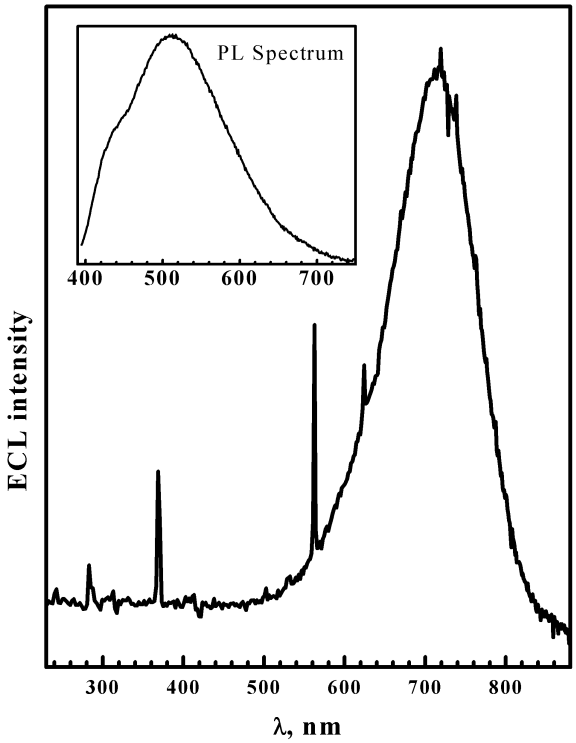

Fig. 14 ECL spectrum of Ge NCs in 0.1 M TBAP DMF electrolyte obtained by stepping electrode potential between + 1.5 V and – 2.5 V at 10 Hz rate for 30 min. *Inset*: PL spectrum obtained from the Ge NCs dispersed in $CHCl_3$. Excitation wavelength: 380 nm [66]

wavelength, which is ~ 200 nm red-shifted compared with the PL spectrum in the inset. This substantial red shift was also observed in the previous experiments with Si and CdSe NCs and is again attributed to surface states of NCs [52, 67].

3.2 Compound Semiconductor NCs

3.2.1 Electrochemistry and ECL of CdS NCs

Monodisperse thioglycerol-capped CdS NCs can be prepared relatively easily and are readily soluble in DMF. The NC sizes are 4.5, 4.3, 4.2, and 3.9 nm respectively from I-IV. The CV response of the stable particles (Q-CdS) is shown in Fig. 15 [54]. Clear oxidation and reduction peaks are apparent at – 2.15 V (A1) and 0.80 V (C1), respectively. The additional peaks only appear on scan reversal after traversing either A1 or C1 (Fig. 15b). Increasing the amount

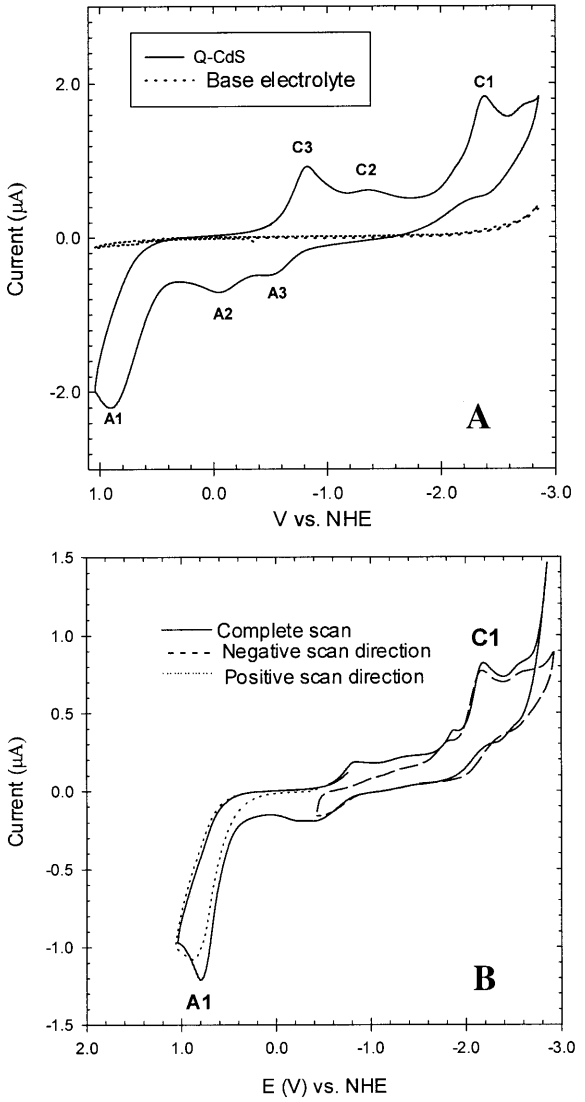

Fig. 15 **a** CV response in the absence and presence of thioglycol-capped CdS Q-particles (1 mg/mL of fraction IV) at a Pt electrode. Sweep rate: 50 mV s^{-1} and [THAP]: 0.05 M. **b** Variation of the initial scan direction for IV illustrating that peaks A2, A3, and C3 are related to C1 and A1; sweep rate: 10 mV s^{-1} [54]

of Q-CdS added resulted in increases in all peak currents without significant shifts in peak potentials. The linear dependence of peak current and potential on the square root of scan rate, ν, from 10 to 500 mVs^{-1} shows that the CV response is due to redox reactions of a solution species rather than an adsorbed film (Fig. 16a) [54]. The peak position shifted with increasing ν, suggesting

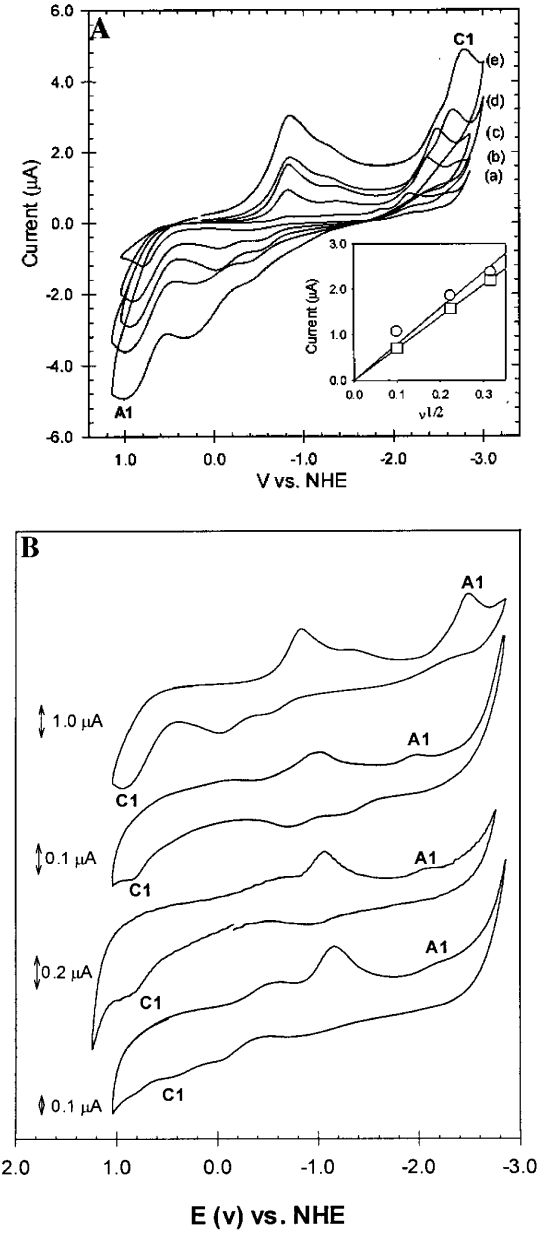

Fig. 16 **a** Scan-rate dependence of the CV response for fraction IV Q-particles at a Pt electrode: *solid line* = 10, 50, 100, 200, and 500 mVs^{-1}. *Inset*: linear dependence of peak currents for A1 (□) and C1 (◯) on $\nu^{1/2}$ (to 100 $mV\,s^{-1}$). [THAP]: 0.05 M. **b** CVs illustrating the electrochemical band gap (A1-C1 peak separation) for fractions I-IV. Particles were added at 1 mg/mL for IV and to the saturation concentration (< 1 mg/mL) for I-III. $\nu = 100\,mV\,s^{-1}$ [54]

kinetic effects. The current response for the other peaks was neither clearly proportional to ν nor $\nu^{1/2}$. The response was stable on repetitive scanning and for several days with no evidence of fouling on either electrode surface.

The peak-to-peak separation between A1 and C1, 2.96 V, is comparable to the 3.23 eV calculated from the electronic spectra (Fig. 17). Thus, these oxidation and reduction peaks can be correlated directly to electron transfer at HOMO and LUMO. The oxidation and reduction reactions are irreversible. An approximate estimate based on the size and diffusion coefficient of the particles suggests the passage of ca. 50 electrons/particle at the peak potentials. In light of this electrochemical behavior, an $(EC)^n$ reaction mechanism was proposed: a multielectron transfer process where the electrons are consumed by fast coupled chemical reactions due to decomposition of the cluster. Essentially, the electron is scavenged immediately after injection into the particle, and unlike the case for Si NCs, the Q-CdS can accept additional electrons at the same potential, giving rise to higher peak currents. The appearance of additional cathodic and anodic peaks in the middle of the potential window (A2, A3, C2, and C3 in Fig. 15a) support this proposition. As illustrated in Fig. 15b, CVs recorded where the initial potential and direction of the scan

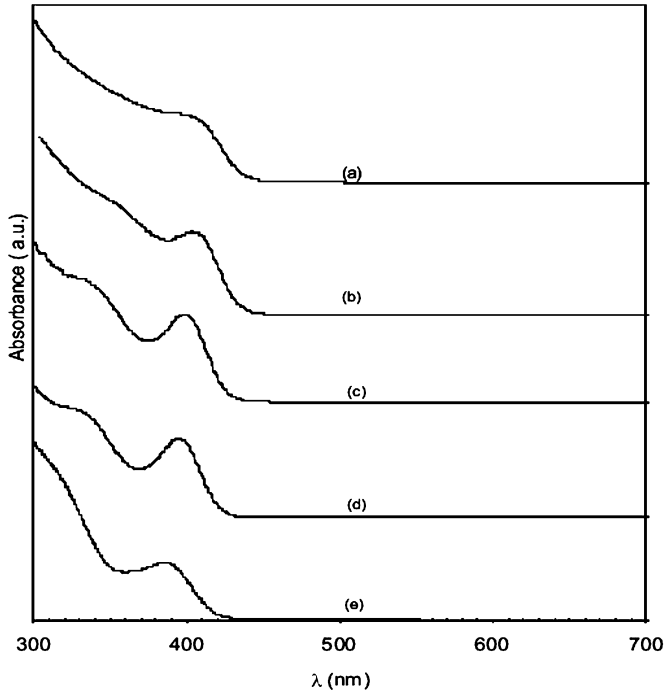

Fig. 17 Comparison of the absorption spectra for Q-CdS in DMF pre- **a** and post- **b**–**e** size selection: **a** "as prepared" NCs and **b**–**e** size selected fractions (I–IV). As expected, the absorption peak is blue-shifted as particle size decreases from **a**–**e** [54]

were varied show that C1 reduction products are reoxidized at A2 and A3. Similarly, C2 and C3 are due to the reduction of oxidation products of CdS at A1. These can be tentatively be assigned to CdS/Cd^0 and CdS/S^0 couples. The small shoulder apparent at ca. – 1.8 V was insignificant at $\nu > 10$ mV s^{-1} (Fig. 16a) and was, thus, neglected. This decomposition upon charge transfer to the particle might be considered equivalent to the trapping of electrons (as Cd^0 for example) and holes (as S for example) on the particle surface. Similar results were observed for PbS [26]. Thus, unlike quantized Si NCs, Q-CdS is reactive and undergoes decomposition upon charging, acting as a source or sink of a large number of electrons at a single potential. To observe discreet charging, semiconductor Q-particles need to be sufficiently stable to undergo electron transfer without the associated following chemical reactions [52].

As the optical band gap is a function of particle size (Fig. 17), the electrochemical band gap should also decrease with increasing particle size, as seen from Table 1 [54]. On a qualitative level, the A1-C1 peak separations decreased with increasing particle size as predicted (Fig. 16b and Table 1). The electrochemical band gap obtained for these fractions is less than the optical band gap. The origin of this difference is probably the rapid following reactions, which cause the peaks to shift to less extreme potentials, as well as the fact that the electrochemical experiments probe surface levels. From the above studies, it was concluded that Q-CdS can act as multi-electron donors or acceptors at a given potential due to trapping of holes and electrons within the particle.

Similar ECL experiments described in Sect. 3.1.1 were carried out using the above CdS NCs, but no perceptible ECL signal was observed in our group because the intermediate species were not stable. However, very recently Ren et al. reported observing ECL from CdS spherical assemblies consisting of 5 nm CdS uncapped NCs [68]. The ECL spectrum showed a peak wavelength of 700 nm.

Table 1 Correlation of optical and electrochemical bandgaps for fractions I–IV where ΔE refers to the peak separation between A1 and C1

Fraction	ΔE (V)[1]	ΔE (V)[2]	Bandgap (eV)[3]	Size (nm)[4]
I	–*	2.63	3.06	4.5
II	2.47	2.98	3.10	4.3
III	2.53	2.88	3.13	4.2
IV	2.96	3.39	3.23	3.9

[1] C1-A1 peak separation at 10 mV s^{-1}
[2] C1-A1 peak separation at 100 mV s^{-1}
[3] Estimated from UV-vis absorption peaks
[4] Estimated from electronic spectra
* Peak not well defined

3.2.2
Electrochemistry and ECL of CdSe NCs

Although there have been several reports on the electrochromic behavior of CdSe NCs, no electrochemical data were reported for CdSe NCs, except for a thin film study by Guyot-Sionnest [69]. In that report, quantitative electrochemical responses from the CdSe NC thin films, which were prepared using cross-linking molecules such as 3-mercaptopropyltrimethoxysilane and 1,6-hexanedithiol, was reported. The electrochromic kinetics and the stabilities of the films treated with cross-linkers were substantially improved compared with the film prepared simply by drying on an ITO or Pt electrode. On the other hand, ECL from solutions of compound semiconductors such as CdS and CdSe NCs have not been reported mainly due to their low solubility and the instabilities of the oxidized and reduced forms [54].

Fig. 18 shows the well-known quantum size effect, in which the absorption edges of CdSe are shifted to higher energies (2.3 eV) from the bulk band gap

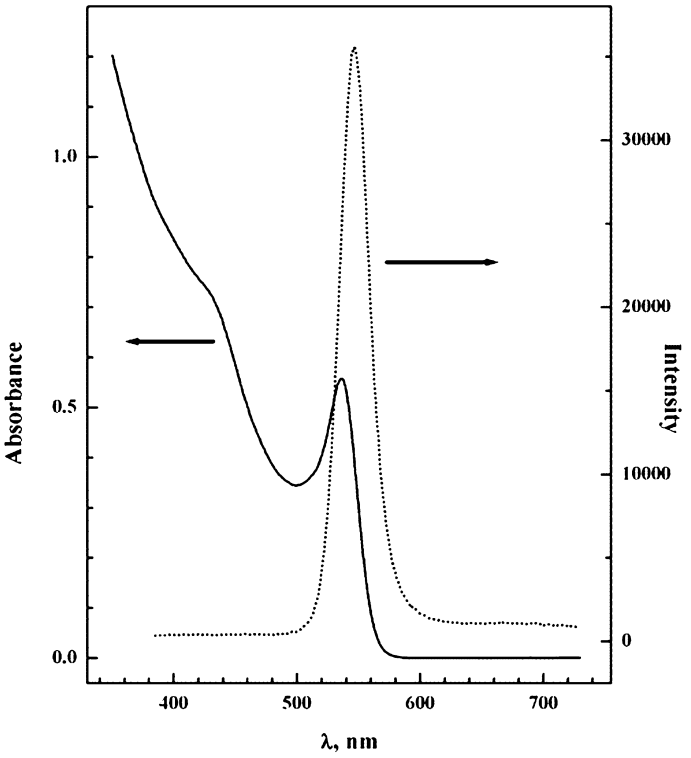

Fig. 18 Room temperature absorption (*solid line*) and emission (*dotted line*) spectra of CdSe NCs dispersed in $CHCl_3$. Excitation wavelength: 370 nm [67]

of 1.7 eV (730 nm) as the particle size decreases [67]. The UV spectrum with the absorption maximum at 537 nm (gap, 2.3 eV) allows one to estimate the size of CdSe NCs as about 32 Å [20]. The PL spectrum shows a non-zero tail towards longer wavelengths, suggesting the presence of surface traps which play an important role in ECL [20, 70].

Unlike the thioglycerol-capped CdS NCs, light emission was observed from the TOPO-capped CdSe NCs in CH_2Cl_2 solution containing 0.1 M TBAP through the annihilation mechanism when the electrode potential was cycled between + 2.3 V and – 2.3 V at a scan rate of 1 V/s (Fig. 19) [67]. As shown in the Figure, ECL light was generated in the potential region that corresponded

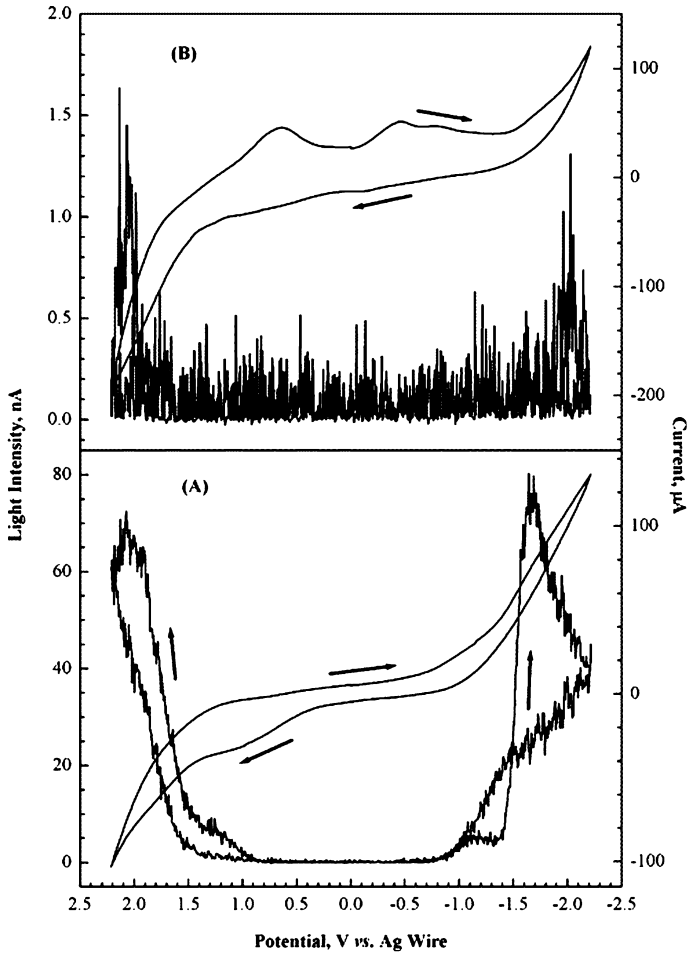

Fig. 19 Cyclic voltammograms and ECL curves of **a** CdSe NCs in 0.1 M TBAP CH_2Cl_2 electrolytes and **b** the blank supporting electrolyte (scan rate: 1 V/s) [67]

to the band gap of CdSe NCs; the threshold voltage ($\sim$ 2.3 V) is almost the same as the optical band gap estimated from the absorption maximum in Fig. 18. Unlike the CdS NCs, electrochemical experiments such as CV and DPV did not show any significant electrochemical features due to the low NP concentration resulting from the limited solubility of the NCs in the solvents employed [54], which made discerning faradaic current from CdSe reactions from the background current difficult.

Some ECL light, generated through the so-called preannihilation mechanism in Fig. 20 [42], was observed. Only oxidized species could be generated in

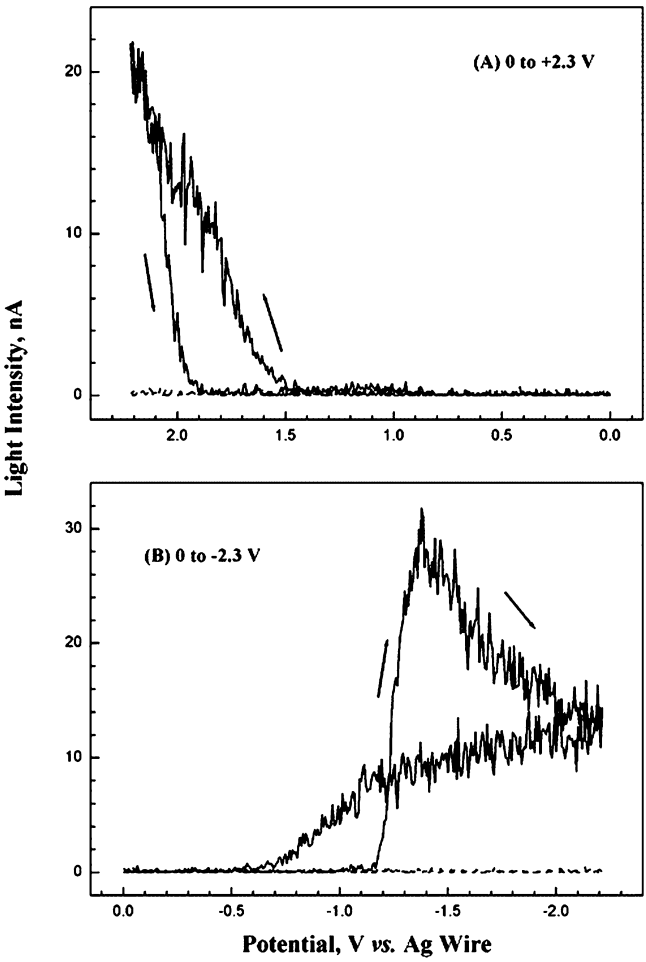

Fig. 20 ECL curves of CdSe NCs in 0.1 M TBAP CH_2Cl_2 electrolytes with a different potential window ("half scan") between **a** 0.0 V and + 2.3 V, and **b** 0.0 V and – 2.3 V (scan rate: 1 V/s). *Dotted curves* are the ECL responses from the blank electrolyte [67]

the "half scan" from 0.0 V to + 2.3 V, but ECL light was observed. Very similar behavior was found for a scan from 0.0 V to – 2.3 V. The origin of this ECL is unclear, but may depend on the presence of impurities or reaction products that can act as coreactants.

Fig. 21a shows ECL transients for annihilation in a double potential step experiment in which the potential was stepped from 0.0 V to – 2.3 V and between – 2.3 V and + 2.3 V. As in the potential scan experiments, the light

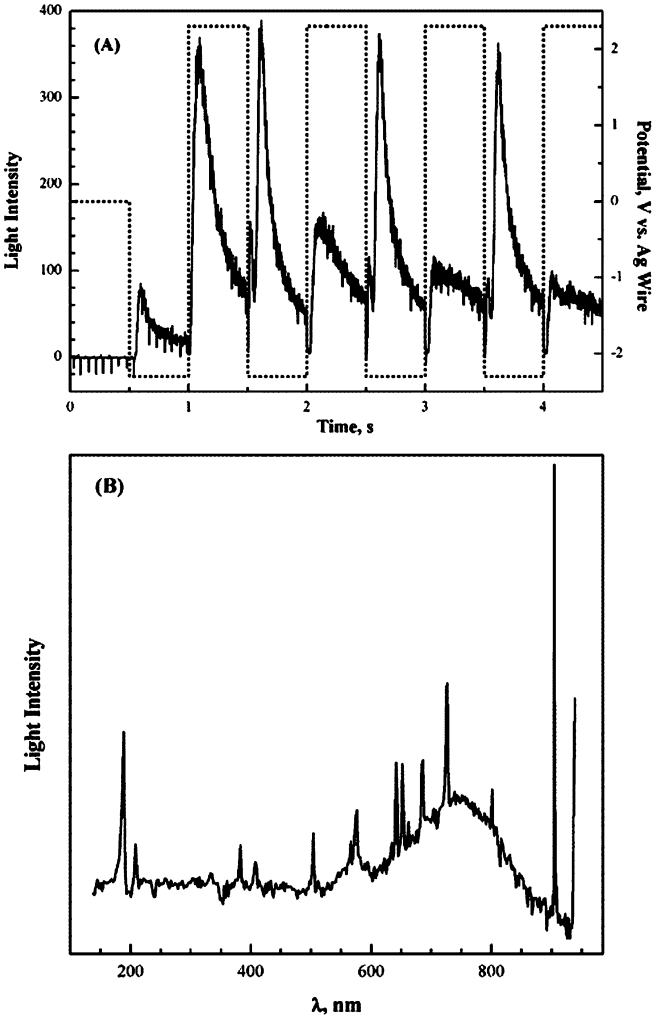

Fig. 21 **a** ECL transients of CdSe (*solid curve*) applied potential steps between + 2.3 V and – 2.3 V (*dotted lines*). **b** ECL spectrum obtained by stepping same potential as in **a** at 10 Hz with an integration time of 30 min [67]

intensity was higher in the potential region where reduced forms were electrogenerated, whereas light intensity in the anodic region decreased substantially with successive potential steps. Fig. 21b shows an ECL spectrum from the TOPO-capped CdSe NCs dispersed in a CH_2Cl_2 solution containing 0.1 M TBAP, obtained using a double potential step between + 2.3 V and – 2.3 V at a 10 Hz rate integrated over 30 min. The observed maximum wavelength at ~ 740 nm is red-shifted by almost 200 nm from that in Fig. 18. This substantial red shift between the PL and ECL emission was also observed in the previous experiment with Si NCs [52]. Because of the high surface to volume ratio of NCs, surface properties have significant effects on structural and optical properties such as emission efficiency and spectrum [70, 71]. For example, adatoms and surface vacancies can provide localized surface states within the band gap. In addition, ECL depends more sensitively on surface states than PL, which mainly occurs through excitation and emission within the NCs core [52]. NC cores have band gaps greater than the energy separation of surface states. Considering all of these factors and the non-zero tail in the PL spectrum shown in Fig. 18, the difference in light emission spectra between ECL and PL most likely results from a major contribution of the surface states in ECL emission. This result suggests the importance of surface passivation studies on ECL.

DPV of 2.5 nm-diameter CdSe NCs was recently carried out [72]. NC reduction in the negative bias region, as shown in Fig. 22, was characterized by a doublet and then a continuous increase in current with applied potential becoming more negative, indicative of two discrete charge transfers followed by multiple charge transfers. The DPV responses in this region reveal information about the conduction levels and look very similar to the tunneling

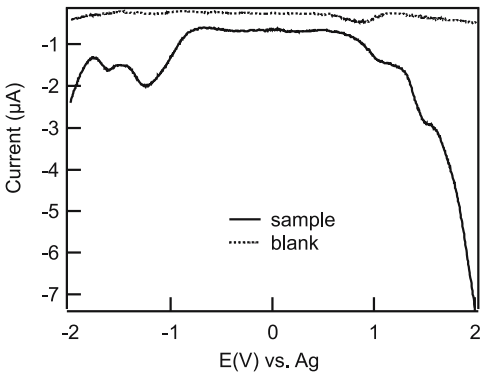

Fig. 22 Differential pulse voltammograms of a dichloromethane solution containing 0.1 M tetrabutylammonium perchlorate (TBAP) as supporting electrolyte (*dotted line*) and 2.50 nm CdSe NCs (40 mM) dispersed in the same solution (*solid line*) at a 0.07 cm^2 Pt disk working electrode with a scan toward positive potential, a scan rate of 20 mV/s and a pulse amplitude of 50 mV [72]

current–voltage spectrum (TCVS) of a CdSe dot of a similar size observed at 4.2 K, obtained by Alperson et al. [73]. The doublet was assigned to the two consecutive electron injections to the first conduction band, $1\,S_e$ (s character) in the case of electrochemically-prepared dots [73]. The energy difference between the first two peaks (the Coulomb charging) was 0.37 eV in DPV, which agrees well with the value in the TCVS (0.34 eV). Broader peaks were observed in DPV than those observed in the TCVS. While the CdSe NCs were monodisperse in size, the broadness of the peaks might be due to the surface states, which increase the complexity of the electronic structure. Furthermore, a continuous increase in current instead of a Coulomb staircase for the following electron injections to the second conduction band was observed in DPV. On the other hand, two oxidation (hole injection) peaks were seen in the positive bias side of the DPV in Fig. 22. These peaks were broader and the Coulomb charging energy was larger (0.48 eV) than that of the negative side. These results were expected due to the higher density of valence levels and the close proximity between Coulomb charging, level spacing as well as the multiplicity of the electronic structures.

The electrochemical gap was determined to be 2.34 eV from the separation of the first oxidation and reduction peaks in the DPV (Fig. 22). This is in good agreement with the optical band gap, 2.50 eV and 2.06 eV estimated from the absorption onset and the broad PL peak of the NC, respectively [72]. The zero current gap in TCVS, 2.88 to 3.13 eV, also provided a qualitative description of the band gap [73]. The electrochemical gap is strongly affected by the presence of surface states that can act as local traps for electrons and holes. We estimate that for NCs of this size, 30% to 50% of the CdSe is on the surface, which may be capped with TOPO or possibly a small amount of oxide. All this evidence suggests that the observed oxidation and reduction may largely reflect the properties of the NC surface. Electron and hole injections may first occur on the 1Se and 1VB bands of surface CdSe respectively. However, the DPV does not clarify where further charge injections occur. In addition, forward and reverse (not shown) DPV scans are relatively less symmetric than those of Si NCs, indicating that charge transfers are not very reversible.

The ECL of the same CdSe used for the above experiments was investigated by recording voltammetric photocurrent with a photomultiplier tube (PMT). ECL was observed under various stimulus conditions. Light emission was produced from both negative and positive sides when the applied potential was swept between – 2.30 and 2.30 V. An annihilation mechanism (electron transfer between reduced and oxidized NCs) was assumed in this light emission process. More interestingly, a significant ECL signal was detected as the potential was scanned from 0.00 to – 3.00 V [72]. The ECL-potential curve showed two overlapping peaks, which may correspond to two emission processes. The ECL turn-on potential was at – 1.30 V, which is slightly more negative than the first reduction peak in DPV. Stable ECL could be obtained by using pseudo-constant potentials, slowly scanning from – 1.60 to – 1.80 V

or from – 2.00 to – 2.20 V. The second peak on the ECL–potential curve appeared at – 2.12 V. Note that in these cases, only the reduced species existed in the solution, and the annihilation leading to light emission could not happen. Therefore, there must be another oxidant that accepted an electron from the valance band of anion NC radicals to form excited states. This coreactant mechanism was interpreted by Bae et al. in the study of CdTe NCs in the same supporting electrolyte, which will be described in the next section [74].

Typical ECL spectra are shown in Fig. 23. The integration time for the spectra is 6 min. As the potential was scanned from 0 to – 2.20 V, the ECL spectrum, consisting of two peaks at 1.90 and 2.55 eV, was very broad and weak. However, strong ECL at 1.90 eV (red, 653 nm) was observed at potentials that were slowly scanned between – 1.60 and – 1.80 V. Even stronger

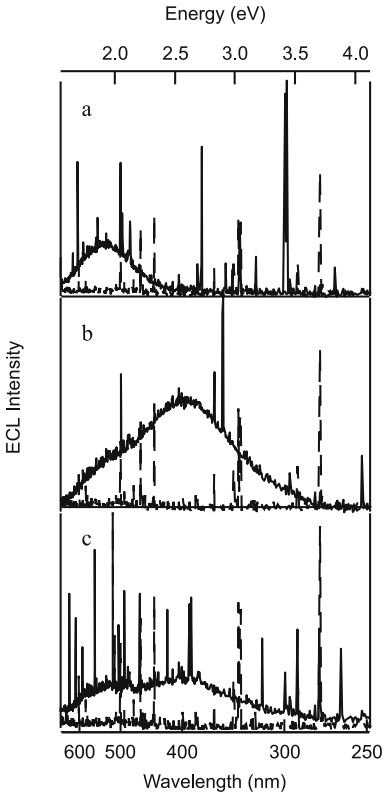

Fig. 23 ECL spectra of 40 μM CdSe NCs in CH_2Cl_2 containing 0.1 M TBAP at a 0.07 cm^2 Pt working electrode, obtained by scanning applied potential between – 1.60 and – 1.80 V **a**, – 2.00 and – 2.20 V **b**, 0 and – 2.20 V **c**. All potentials are referred to Ag wire. Scan rates for **a**, **b** and **c** were at 10, 10 and 500 mV/s. An integration time of 6 min was used. *Dotted curves* represent the responses of corresponding blank supporting electrolyte solutions recorded at the same conditions. *Vertical lines* are cosmic rays on the CCD camera [72]

ECL, consisting of two peaks at 1.90 and 2.55 eV (blue, 486 nm), was emitted at more negative potentials (– 2.00 to – 2.20 V). It was assumed that ECL at 1.90 and 2.55 eV correspond to the surface state and core structure emission respectively, because these energies are in good agreement with band gaps from surface and core electronic structures as analyzed from the electrochemical and spectroscopic study. Emission at 2.55 eV implies that the current rise at very negative potentials in DPV resulted from electron injection to the core conduction band. Quantitatively, however, it is not clear why the NCs luminesced at 1.90 eV simultaneously when stimulated with higher energy. It is even more difficult to understand at this point why ECL was only observed at a longer wavelength (1.70 eV) for 3.2 nm-diameter CdSe NCs prepared using similar methods in a previous report, which was discussed above [67]. It can be speculated that ECL from the core was not favorable in the absence of oxygen molecules in an airtight electrochemical cell. Another aspect is that NCs were obtained with different crystallinity from that of the NCs in the previous report [67], which lead to different crystal band structures. Bawendi et al. [20] found that simulated X-ray powder diffraction spectra for 3.5 nm-diameter spherical nanocrystallites such as zinc blende, wurtzite and wurtzite with one stacking fault are very different. However, more detailed study is needed to derive the relationship between nanocrystallinity and the ECL. The results demonstrate the ability of the NCs to yield light emission tunable by the applied potential.

ECL from CdSe NCs capped by octadecanamine (ODA) with diameters of 2.31, 2.45 and 2.65 nm (samples 1, 2 and 3) was investigated by Zhou et al. [75]. ECL spectra of these different sized NCs at the optimized stimulus conditions are shown in Fig. 24. It can be seen that ECL for sample 1 is relatively strong and has a peak wavelength at 510 nm, which is identical to that in PL spectrum [75]. ECL is weak for samples 2 and 3 and shows a peak position at 663 nm, which is red shifted more than 100 nm from the peak wavelength of PL spectra.

It was expected that the ECL peak wavelength of CdSe NCs with a direct bandgap would be blueshifted with decreasing NC size. Though the anticipated size-dependent feature of ECL is not apparent in Fig. 24, two colors of ECL were obtained from the prepared NCs. NCs of very small size can have totally different optical properties in this special environment [73], sample 1, with possibly richer surface states. These would produce an ECL spectrum that includes both core and surface trap emission, which is in contrast to the conventional situation. This phenomenon provided a good opportunity to study the fate of injected electrons and holes in the NCs in the presence of surface states. It is reasonable to attribute this result to the crystal structure change occurring in the small-sized NCs. The structural change may trigger electronic structure reorganization, which would allow the core level to accept the injected electrons and holes. Also, it is possible that because of the space effect of the ligand, small NCs have a greater chance of colliding with the co-

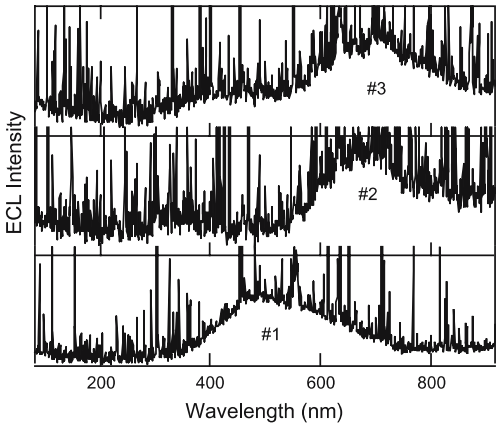

Fig. 24 ECL spectra of 2.5 μM CdSe solution in CH_2Cl_2 with 0.1 M TBAP. Scanning potential windows are – 1.0 to – 2.8 V for samples 1 (2.31 nm) and 2 (2.45 nm) and 2.5 to 3 V for sample 3 (2.65 nm). Scan rate is 0.5 V/s and integration time is 30 min. *Vertical lines* are cosmic rays from the CCD spectrometers [75]

reactant directly, thus allowing the injection of a hole to produce the exited state.

The aging method was explored in order to enhance the ECL intensity. The above three electrolyte solutions were kept in the dark for two months and their ECL were tested under the same conditions. The NCs showed much better (sharper and clearer) ECL spectra, which are illustrated in Fig. 25. After

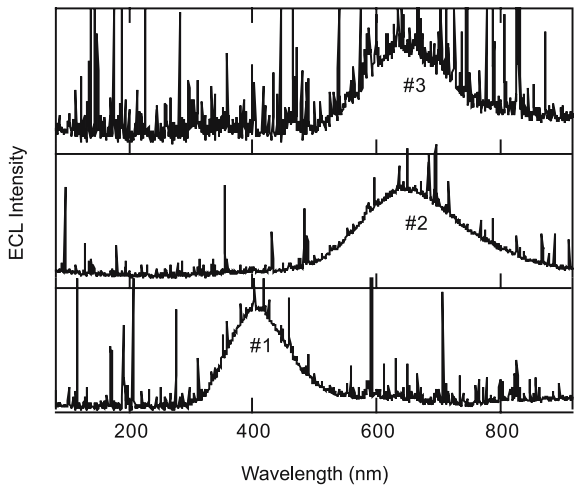

Fig. 25 ECL spectrum of aged CdSe solution in CH_2Cl_2 with 0.1 M TBAP. Other experimental conditions are the same as those in Fig. 24 [75]

aging, samples 2 and 3 showed an ECL enhancement effect. This agrees well with the fact that the PL yields of CdS/dendrimer nanocomposites continuously increased with aging [76]. In fact, CdSe NCs were in self-focusing growth during the aging process. The ECL enhancement is ascribed to an optimal surface structure reconstruction, which may lead to less quenching of luminescence. Sample 1 produced not only a sharp and clear emission but was also blueshifted by 100 nm, which suggests the possibility of NC reconstruction and size focusing. However, further work is required to establish exact mechanisms for ECL intensity enhancement.

3.2.3 ECL of CdSe/ZnSe NCs

The PL efficiencies of NCs are sensitive to the nature of the particle surface; surface states act as quenchers of the luminescence [52, 67]. Passivation of the surface is the key to preparing highly luminescent semiconductor NCs for use in light-emitting devices and tagging applications [78–80]. Such surface passivation has been achieved using organic capping agents as well as by forming inorganic core/shell systems such as in CdSe/ZnSe [29, 70, 77, 78, 80, 81].

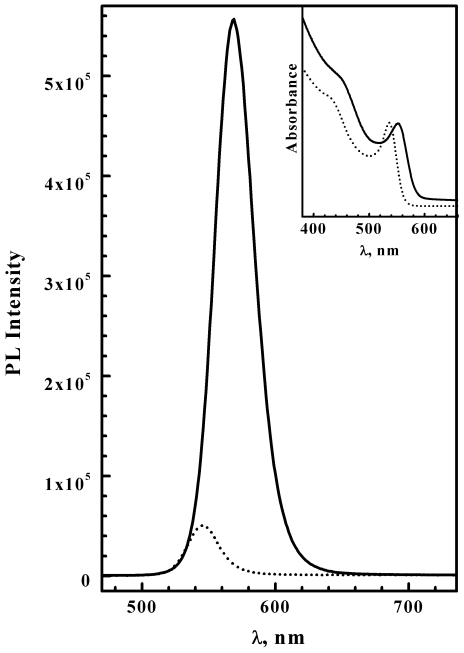

Fig. 26 PL and UV absorption (*inset*) spectra of CdSe (*dotted line*) and CdSe/ZnSe (*solid line*) NCs dispersed in $CHCl_3$. Excitation wavelength: 370 nm [77]

As discussed, the ECL emission is characteristic of surface energy levels, while the PL is dominated by excitation and emission within the NC core [67]. Therefore, highly passivated NCs should result in an ECL spectrum that is more like the PL spectrum.

The formation of a core/shell structure results in a dramatic enhancement of PL. Fig. 26 shows PL and UV absorption spectra (inset) of CdSe/ZnSe NCs dispersed in $CHCl_3$. As shown, both the PL and UV spectra from the core/shell NCs essentially maintain their overall shape, with a small redshift compared to those of CdSe NCs, which is an indication of the formation of core-shell structure [78, 79, 81]. Also, the PL peak intensity after passivation with a shell of ZnSe NCs increased by more than ten times, compared to CdSe, without significantly modifying the absorbance and PL features.

As discussed earlier, the ECL spectrum from Si and CdSe NCs showed a significant redshift from the PL, which was attributed to surface effects [52, 67]. Fig. 27 shows an ECL spectrum from the CdSe/ZnSe NCs dis-

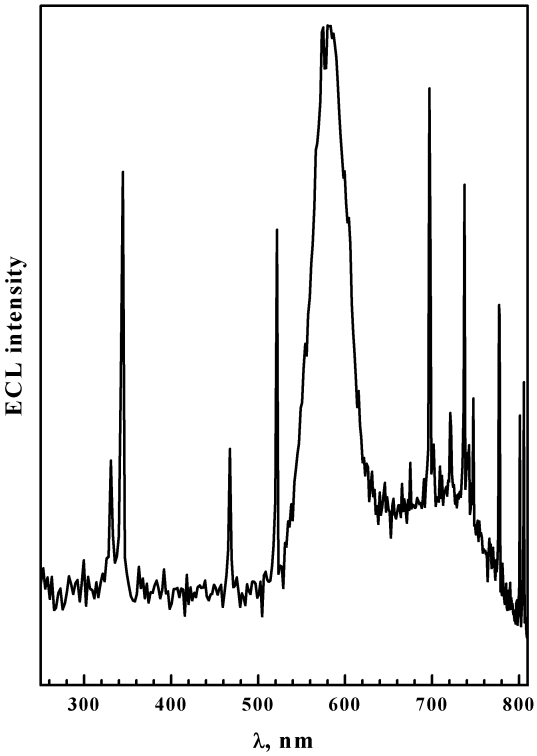

Fig. 27 ECL spectrum of CdSe/ZnSe core-shell NCs in a CH_2Cl_2 solution containing 0.1 M TBAP. The spectrum was obtained by stepping the potential between + 2.3 V and – 2.3 V at 10 Hz, with an integration time of 30 min. The large sharp peaks represent random cosmic ray events detected by the CCD camera [77]

persed in a CH_2Cl_2 solution containing 0.1 M TBAP. This ECL spectrum shows one main peak at ~ 580 nm, which is almost identical to that in the PL spectrum (Fig. 26). In other words, the redshift observed with CdSe has been largely removed, indicating that the solution contains NCs whose surfaces have been largely passivated. There is another broad peak at ~ 740 nm, which is redshifted by ~ 200 nm from the PL peak. This is the same degree of redshift as found in the ECL spectra from CdSe and Si NCs [52, 67]. This broad and ill-defined peak thus results from those NCs whose surface is not passivated, suggesting that passivated CdSe NCs are present together with some non-passivated NCs. This ability to probe the surface states of NCs is an important advantage of ECL.

3.2.4
Electrochemistry and ECL of CdTe NCs

Figure 28 shows DPVs of two different batches of CdTe NCs [74]. In Fig. 28a, in a 5 : 1 (v/v) benzene/acetonitrile mixture as a solvent, three anodic peaks (A1 and A2 at 0.45 and 0.73 V with a potential spacing of 0.28 V and an additional peak at 0.9 V) were observed in the positive potential scan. Three cathodic peaks (C1 at – 1.68 V and two other peaks at – 1.0 and – 1.24 V) appear in the negative potential scan direction. The first anodic peak (A1) is characteristic of a one-electron reaction and was sometimes difficult to distinguish from the background, as shown in Fig. 28b, even in the same batch of particles in the same electrolyte solution. The third anodic peak around 0.9 V and two cathodic peaks at potentials more positive than – 1.68 V were not reproducible and are probably due to impurities in the NC preparation or reduction of residual oxygen. The electrochemical band gap between the first cathodic (C1) and anodic (A1) peaks from Fig. 28a is 2.13 V, which is close to the value of 2 eV obtained spectroscopically. Similarly, in Fig. 28b, the electrochemical band gap is ~ 2 eV if the positive onset point or the shoulder near ~ 0.45 V is taken as the first anodic current peak. Recently, Gao and co-workers [82] reported voltammetric current peaks of thioglycolic acid-stabilized CdTe NCs around – 1 and + 1 V (vs. Ag/AgCl) in aqueous solution. Similar voltammetric behavior was observed by Greene and coworkers [83] from a solid film of dimethyldioctadecylammonium-stabilized CdTe NC monolayer. They reported an electrochemical band gap that correlated with the optical value as well as anodic current peaks located at potentials inside the valence band edge, which were explained by hole injection into the surface traps of the particles. The diffusion coefficient of the NCs was estimated as being on the order of 10^{-6} cm^2/s [74]. The electrochemical behaviors of the synthetic precursors, like TOPO, $Cd(ClO_4)_2$, TOP and Te, were also investigated [74].

Figure 29 shows an ECL–potential curve and transients of CdTe NCs in dichloromethane containing 0.1 M $TBAPF_6$. As the potential is scanned from

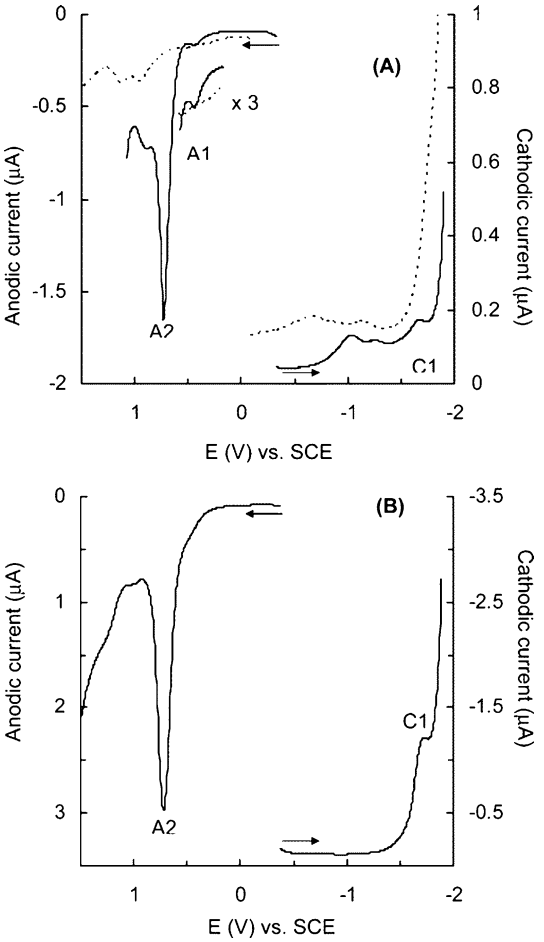

Fig. 28 Differential pulse voltammograms of two different batches of CdTe NCs at a 0.06 cm^2 Pt working electrode, scanning toward positive or negative potentials, at scan rates of 10 mV/s and a pulse amplitude of 50 mV. The *arrows* indicate the starting potential and scan direction. **a** 9.6 μM CdTe NCs in 5 : 1 (v/v) benzene/acetonitrile containing 0.1 M TBAP. The current value of peak A1 is magnified three times and *dotted lines* are background signal from supporting electrolyte solution. **b** 32 μM CdTe NCs in CH_2Cl_2 containing 0.1 M $TBAPF_6$ [74]

0 to – 2.46 V (vs. SCE) at a scan rate of 1 V/s, as shown in Fig. 29a, a significant ECL signal is detected around – 1.85 V, which is slightly to the negative side of the first cathodic DPV peak potential (see Fig. 28), and shows a large peak at a more negative potential. However, in a reverse potential scan, ECL is not observed in the positive potential region. In Fig. 29b, the ECL transients were measured by applying 10 Hz potential steps between – 2.46 and + 1.44 V (*solid line*). A large ECL signal is detected at the first negative poten-

tial step and a much smaller ECL signal at the subsequent positive potential. The latter can be explained by electron transfer reactions between reduced and oxidized NCs. This smaller ECL signal was sometimes undetected, even in ECL transients. The former ECL observed at the first negative potential region cannot be explained by the annihilation of redox species of NCs, because there are only reduced particles; there are no oxidized particles to act as electron acceptors. Instead, the larger ECL signal is still observed by applying negative potential steps from – 0.46 to – 2.46 V in Fig. 29b (*dotted line*). In a different solvent, a mixture of benzene and acetonitrile, the ECL signal

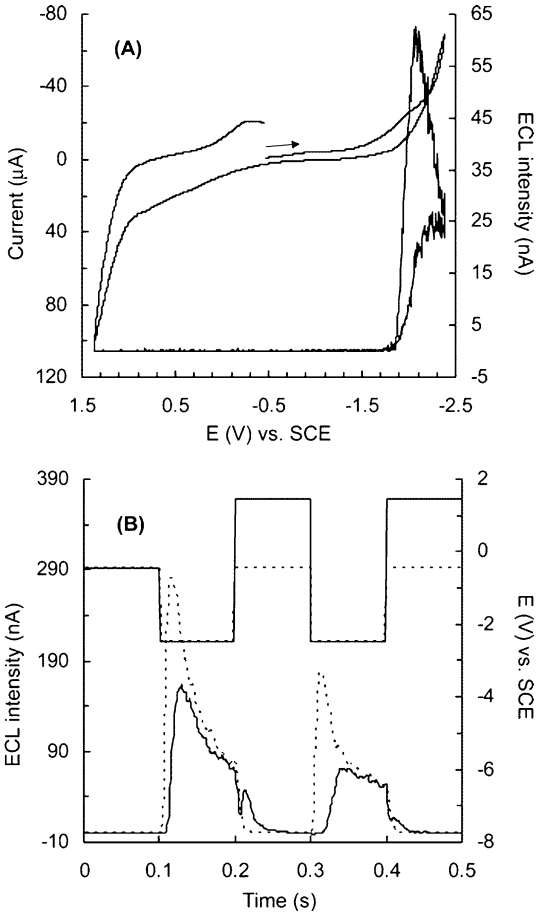

Fig. 29 **a** Cyclic voltammogram and the corresponding ECL potential curve (scan rate: 1 V/s) and **b** ECL transients (*lower curves*) obtained by stepping potential (*upper curves*) between – 2.46 and + 1.44 V (*solid line*) or half potential between – 0.46 and – 2.46 V (*dotted line*) of ~ 7 μM CdTe NCs in CH_2Cl_2 containing 0.1 M $TBAPF_6$ at a 0.06 cm^2 Pt working electrode [74]

was 30 times smaller at the first negative potential, which can be attributed to some impurities in the cell [74]. These results suggest that the large ECL at the first negative potential in Fig. 29 might result from the dichloromethane solvent acting as a coreactant. Ushida and co-workers [84] revealed that $CH_2Cl^{\cdot}$ radicals produced under irradiation of CH_2Cl_2 act as electron acceptors in order to oxidize aromatic hydrocarbons. Based on this reference, $CH_2Cl^{\cdot}$ was proposed as the oxidant in the system. The reduced CH_2Cl_2, $CH_2Cl_2^{-\cdot}$, decomposes into $CH_2Cl^{\cdot}$ and Cl^-, and the oxidant, $CH_2Cl^{\cdot}$, accepts an electron from the reduced NC to form the emitting state.

$$CH_2Cl_2 + e^- \rightarrow CH_2Cl_2^{-\cdot} \rightarrow CH_2Cl^{\cdot} \quad (20)$$

$$(CdSe)_{NC}^{-\cdot} + CH_2Cl_2^- \rightarrow (CdSe)_{NC}^{*} + CH_2Cl^- \quad (21)$$

The CdTe NCs exhibited a unique ECL spectrum (Fig. 30). The ECL peak at 638 nm, which was obtained by stepping potential between – 2.3 and + 2.3 V (vs. Ag wire) at 10 Hz in dichloromethane solvent is very close to the PL maximum at 635 nm. The same ECL peak position was observed by stepping between 0 and – 2.3 V (vs. Ag wire). Fig. 30 suggests that the synthesized CdTe NCs have no deep surface traps causing luminescence at longer wavelength. Even though the CdTe NCs were synthesized by the same procedure used in CdSe NCs with TOPO capping agent, they show a more completely passivated surface than CdSe NPs based on the ECL results. This conclusion is supported by the fact that very small PL tails were observed at longer wavelengths than the wavelength of band-edge PL [74].

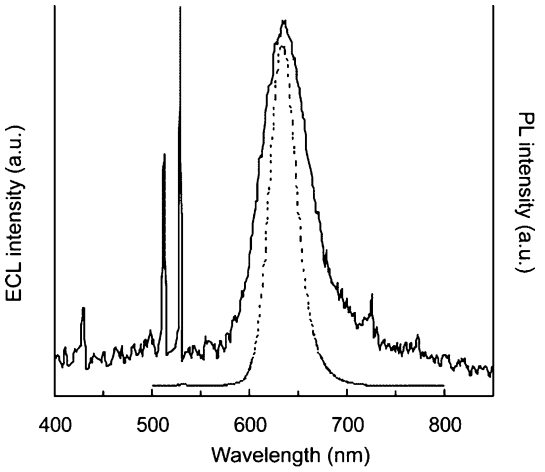

Fig. 30 ECL spectrum (*solid line*) obtained by stepping potential between – 2.3 and + 2.3 V (vs Ag wire) at 10 Hz, with an integration time of 20 min, of ~ 7 μM CdTe NCs in CH_2Cl_2 containing 0.1 M TBAP at a 0.1 cm^2 Pt working electrode. *Dotted curve* is PL spectrum to compare with ECL spectrum [74]

3.2.5
Electrochemical Behavior of PbS NCs

In a recent report on the electrochemical properties of PbS NCs [26], the possibility of QDL was raised to interpret the observed voltammetric response, but, as for CdS NCs, the authors proposed that the peaks observed are instead due to redox reactions coupled with PbS decomposition.

The particles synthesized under particular experimental conditions were denoted as C6-PbS (2*x*), where 2*x* reflects a two-fold molar excess of 1-hexanethiol (C6SH) over Pb. The cyclic voltammograms of the 1-hexanethiol-capped PbS NCs dissolved in freshly distilled CH_2Cl_2 containing 0.10 M TBAP are shown in Fig. 31 [26]. The potential sweeps started at 0 and initially proceeded in the negative direction. Within the potential range of – 1.0 to + 0.8 V, only featureless voltammetric currents (a flat current–potential curve) were seen, and these were interpreted as arising from the band gap of these PbS NCs. This appears to be consistent with the aforementioned UV-VIS and TEM results (1.5–1.8 eV). When the negative potential range was expanded further to – 1.6 V, three pairs of rather well defined waves (labeled I, II, and III) at – 1.3, – 1.0, and – 0.67 V, respectively, were observed (Fig. 31). These three waves showed a modest peak splitting (ranging from 20 to 200 mV), suggesting quasi-reversible electron-transfer processes; the peak potential spacing was almost constant at about 300 mV. At first glance, this appears to be consistent with so-called electrochemical quantized capacitance charging to monolayer-protected nanoparticles such as Au NCs [34], where the par-

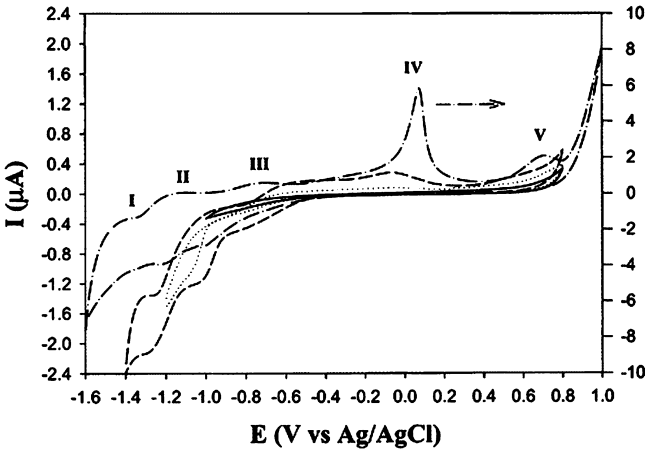

Fig. 31 Cyclic voltammograms of a Pt electrode (0.78 mm^2) in C6-PbS (4*x*) nanoparticles (ca. 0.4 mM) dissolved in freshly distilled CH_2Cl_2 containing 0.10 M tetra-*n*-butylammonium perchlorate (TBAP) within various potential windows. The potential sweeps were always started cathodically, and the potential sweep rate was 100 mV/s [26]

ticle molecules behave as diffusive nanoelectrodes in solution and discrete charging of the particle double-layer results in the appearance of electrochemical analogs of coulomb staircase charging. However, the authors [26, 34] concluded from the capacitance calculation with Eq. 16 and from the electrochemistry of bulk PbS [85, 86] that it is more likely that these voltammetric features are due to cathodic reduction reactions of the PbS NCs, as further supported by the voltammetric responses at an even wider potential window of – 1.6 to + 1.0 V. One can see that, in addition to the three pairs of voltammetric waves observed in the negative potential region, there are two rather well-defined anodic waves observed at + 0.1 and + 0.7 V, respectively (labeled IV and V). In particular, peak IV becomes rather prominent, compared to that observed in the previous potential window (– 1.4 to + 0.8 V). Whereas the detailed reaction mechanism remains largely unknown, the authors proposed that the voltammetric waves (I, II, and III) are related to the reductive decomposition of PbS and Pb-SC6 to Pb and the corresponding sulfur or thiolate [26]:

$$\text{Anodic dissolution} \quad \mathrm{PbS} \rightarrow \mathrm{Pb^{2+}} + \mathrm{S} + 2\,\mathrm{e} \tag{22}$$

The sharp feature of peak IV (at 0.1 V) might reflect the anodic stripping of surface-accumulated Pb. The peak height of IV became more pronounced at a lower potential sweep rate, and the peak position shifted in the positive direction at increasing sweep rate, indicating a kinetically sluggish process. Peak V and the sharply rising anodic current at even more positive potentials might be ascribed to the anodic dissolution of PbS (reaction 22). These faradaic processes gave rise to a rather significant increase in the overall voltammetric currents (Fig. 31).

3.3 NC Films

Semiconductor NCs are a form of "artificial atoms" that may find applications in optoelectronic systems such as LEDs and photovoltaic cells, or as components of future nanoelectronic devices. The behavior of thin films of NCs is of interest to those researching such devices.

3.3.1 Si NCs and Porous Si

The integration of Si-based optical functions with Si electronic functions is of interest. To our knowledge, there are no reports on EL devices based on capped Si NCs. Using the method established for the fabrication of organic LED on ITO [45, 46, 87, 88], capped Si NCs were spin-coated onto an ITO substrate (film thickness about 100 nm). A voltage was then applied to the film between ITO (positive) and a Ga : Sn eutectic (negative) contact. The

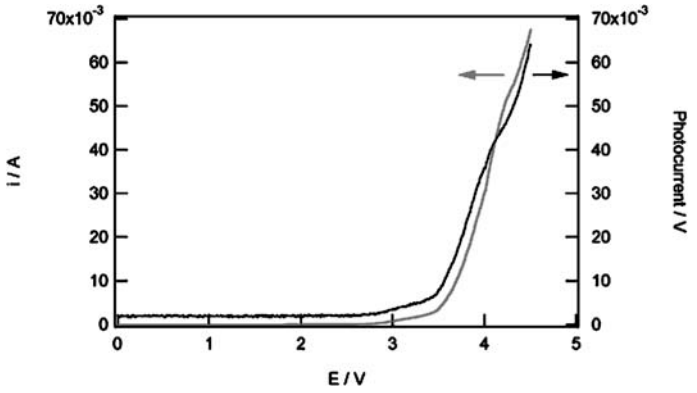

Fig. 32 Current-voltage and luminescence-voltage plots of a thin layer of octanol-capped Si nanoparticles. The voltage scan rate was 50 mV/s [44]

current–voltage and luminescence–voltage plots show a diode-like behavior with a turn-on voltage of 3.0 V (Fig. 32) [44]. The emission mechanism is probably similar to that for the ECL of Si NCs in solution, from the annihilation of electrogenerated holes and electrons hopping from the anode and the cathode and meeting in the film (reactions 8 and 9). A detailed model of analogous EL in solid-state LEDs based on amorphous film of $Ru(bpy)_3(ClO_4)_2$ is presented elsewhere [88]. This preliminary result suggests that by optimizing film preparation conditions, improvements in the emission intensity and efficiency might be possible. A better understanding of the mechanism of operation and the emission decay is also needed.

Studies on LED devices containing porous Si [89] and Si nanowires [90] have been reported and reviewed [91].

3.3.2 PbSe Film

Electrochemistry can be used to dope QDs, both *n*- and *p*-type, and may be useful in the fabrication of several novel optoelectronic devices. A spectroelectrochemical technique monitoring the visible and the IR absorption was applied to a film of 7.2 nm-diameter PbSe NCs in order to determine the number of charges injected into the NCs and to distinguish charges injected into delocalized quantum confined states from those in localized trap states [92]. PbSe NCs have a small band gap (since bulk PbSe has a gap of 0.278 eV at 298 K) and should be able to bring both hole and electronic states into the range of stable electrochemical charge injection. Fig. 33 shows that the first exciton (1Sh-1Se) at 5100 cm^{-1} and the second exciton (1Ph-1Se) at approximately 6600 cm^{-1} are bleached and the intraband (1Se-1Pe) transition at around 1500 cm^{-1} turns on. At positive potentials, holes occupy the 1Sh

state, causing a bleaching of the interband transitions involving that state and inducing intraband absorptions to higher energy hole states in the valence band. At + 0.55 V, Fig. 33 shows the bleaching of the first exciton (1Sh-1Se) and the second exciton (1Sh-1Pe) around 6500 cm^{-1}. These bleaching features are accompanied by an induced absorption feature at around 1400 cm^{-1}, assigned to the 1Sh-1Ph intraband transition. Because of the similarity in the effective masses of the electrons and the holes, the electrochromic effects of hole and electron injection appear strikingly similar, with only small shifts in the energies of the transitions.

Figure 34 plots the magnitude of the bleaching of the first exciton, 4400 cm^{-1}, versus the potential applied to a film of 8.8 nm diameter dots. Also shown in Fig. 34 is the CV of the same sample, which shows no variation over several cycles. At potentials more negative than – 0.725 V 100% bleaching of the first exciton is observed. This corresponds to the filling of the 1Se state in all of the QDs in the film. For this sample, the bleach of the first exciton due to hole injection plateaus at ~ 90%. The application of more positive potentials causes irreversible changes to the film. The voltammetry shows a much more reversible feature for the reduction than for the oxidation, consistent with the lower stability of the injected hole. Similar behavior is observed for films of 7.2 nm-diameter PbSe NCs; however, for those dots, hole injection bleached the first exciton by ~ 75%. For dots smaller than those two sizes mentioned here, no significant hole injection was observed, although electron injection

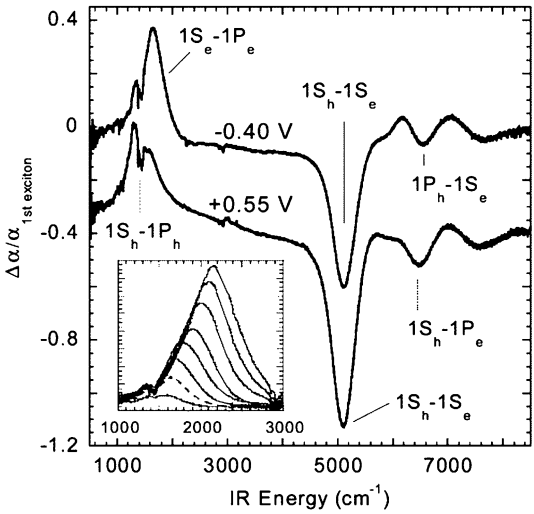

Fig. 33 Difference spectra for a film of 7.2 nm diameter PbSe dots at – 0.40 and + 0.55 V, offset for clarity. The *inset* shows the induced absorption for a series of voltages between – 0.35 and – 0.70 V; the *dotted line* is the feature at – 0.40 V. Solvent absorption peaks in the 1000–2000 cm^{-1} range disrupt the induced absorption feature [92]

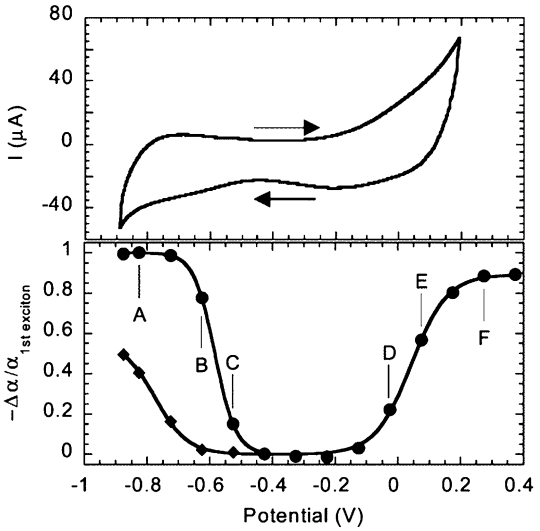

Fig. 34 The *top panel* shows the CV for a film of 8.8 nm-diameter PbSe QDs at a scan rate of 17 mV/s. The *bottom panel* shows the normalized optical bleaching of the first (●) and third (■) excitons, as a function of the applied potential [92]

was still possible. Injection of charge carriers into higher energy states was only observed for electrons. The magnitude of the bleaching of the third exciton (1Ph-1Pe) is plotted as a function of the applied potential in Fig. 34.

3.3.3 CdSe NC Thin Film and Single Monolayers of CdSe in Molecular Organic Devices

Guyot-Sionnest et al. have recently reported that the color of colloidal CdSe NCs is highly controllable electrochemically, a direct consequence of quantum confinement on the electronic states [62, 63]. Electron injection into CdSe NC thin films was reversibly controlled by applying an electrochemical potential [94]. Complete bleaching of the visible interband transition and strong mid-IR intraband absorption was observed upon electron injection into CdSe NC films. The electrochromic response was fairly reproducible; however, complete color change and recovery took hundreds of seconds [94]. Moreover, as shown in Fig. 35 [69], the recovery was fairly slow.

TOPO-capped CdSe NC thin films exhibit stable and quantitative electrochemical responses when treated with cross-linking molecules such as dithiols or diamines (Fig. 36). For a 100 nm-thick film of 6.2 nm-diameter NCs, the electrochromic changes were 1000-fold faster (on the 100 ms timescale), and remained reproducible after 10 000 cycles (Fig. 37) [69], 0.15 at the peak exciton. The color switching is easily observed by eye.

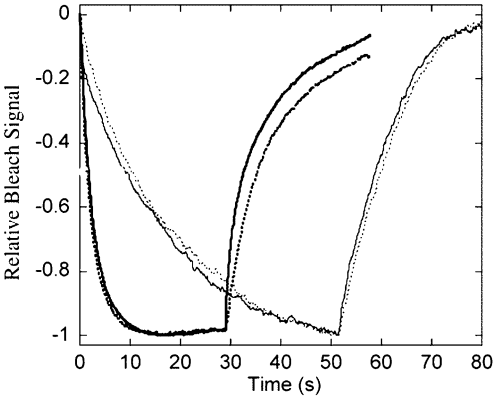

Fig. 35 Time trace of the bleaching and recovery of 6.2 nm diameter CdSe NC films on an ITO electrode. The optical signal is measured at 639.5 nm, and all bleaching signals are normalized to – 1. The *solid lines* are for a negative potential step followed by a return of the potential to 0 V with respect to the Ag quasi-reference. The *dotted lines* are for the same negative potential step followed by the electrode being disconnected. *Fine line*, TOPO-capped CdSe; *heavy line*, pyridine-capped CdSe [69]

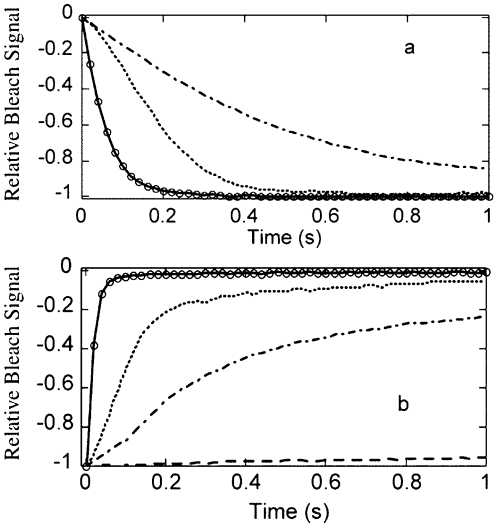

Fig. 36 Time trace of the bleaching **a** for different films of 6.2 nm diameter CdSe NCs on an ITO electrode after the negative potential step, and recovery **b** after returning the potential to 0 V with respect to the Ag quasi-reference. The optical signal is measured at 639.5 nm, and all bleaching signals are normalized to – 1. The solid line and data points are for pyridine-capped NCs treated with 1,6-hexanedithiol. The *dotted line* is for pyridine-capped NCs treated with 4,4′-biphenyldithiol. The dot-dashed line is for TOPO-capped NCs treated with 4,4′-biphenyldithiol. In **b**, the dashed line shows the much slower bleaching recovery for a film of pyridine-capped NCs treated with 1,6-hexanedithiol when the electrode is disconnected [69]

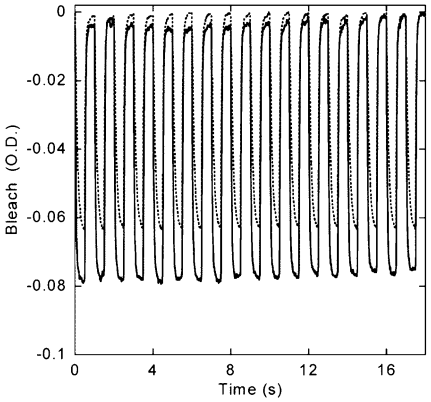

Fig. 37 Optical density at 639.5 nm for a 6.2 nm diameter pyridine-capped NC film cross-linked with 1,6-hexanedithiol on an ITO electrode while cycling the electrode between – 0.8 V and – 1.4 V with respect to the Ag pseudo-reference. The *solid line* is the electrochromic response of the thin film for the first few cycles. The *dotted line* is the response after about 3 h and 10 000 cycles [69]

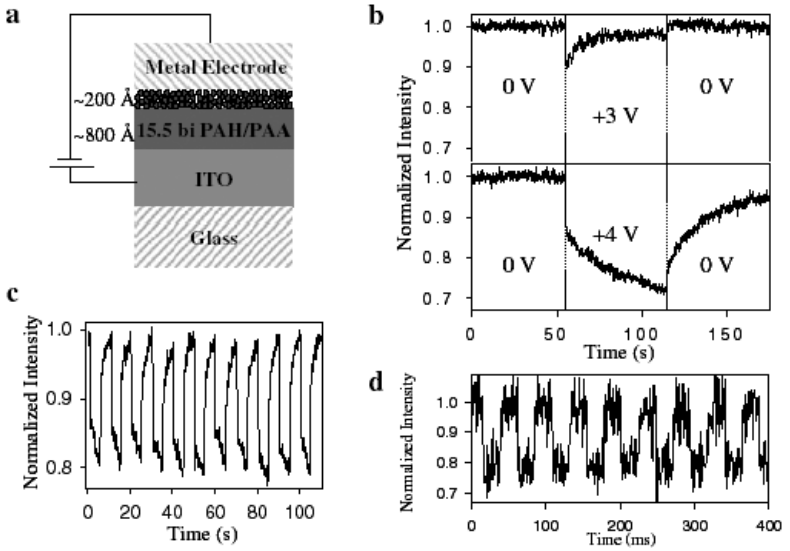

Fig. 38 **a** Schematic diagram of the NC charging device. The insulating layer consists of 15.5 bilayers of PAH/PAA with the PAH layer on top. The ITO serves as a transparent electrode for PL measurement through an optical microscope. The excitation source consists of a continuous wave Ar ion laser (514 nm, 50 W cm^{-2}) and the PL is detected by a CCD camera. Typical working pixel area is 6 mm^2 with eight pixels per device. **b** The charging time-traces for bare, 2.2 nm radius, CdSe NCs with 3×10^5 V cm^{-1} (*top*) and 4×10^5 V cm^{-1} (*bottom*). **c** The photostability of the device is evidenced by the recovery of the PL intensity after the charge/discharge cycling of the voltage sequence. **d** Fast charging and discharging times of a CdSe NC charging device operating under the critical voltage [95]

Bawendi et al. [95] fabricated a simple solid-state device (Fig. 38a) that can reversibly charge multiple layers of CdSe NCs. The device consists of an insulating polymer layer and a thin, spin-coated NC layer sandwiched between two electrodes. A layer-by-layer deposition technique was employed to cast the polyelectrolytes poly(allylamine hydrochloride) and poly(acrylic acid) sequentially onto an ITO electrode [95]. This simple technique resulted in highly uniform thin films with precisely controlled thickness and chemical composition over a large area. Reversible fluorescence quenching and bleaching of the absorption of the NCs were directly observed upon applying a voltage (Fig. 38b–d). The drastic changes in the optical properties led to the suggestion of possible use of NCs in optical modulators and in tunable fluorescent or photochromic displays.

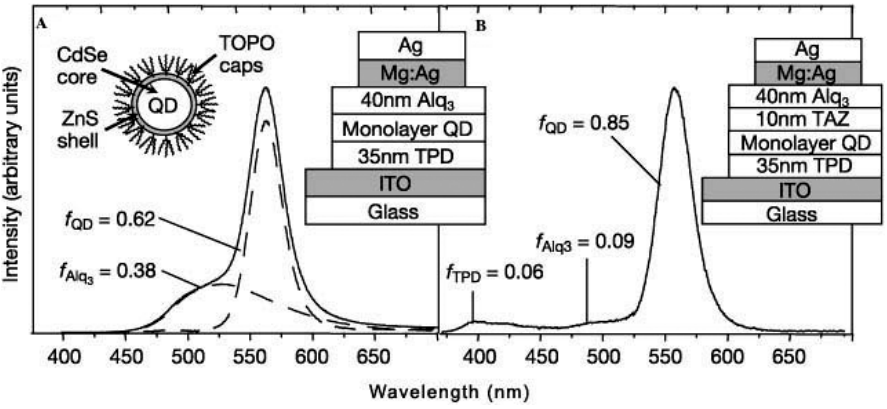

Fig. 39 Electroluminescence spectra and structures for two QD-LEDs, devices I and II. *Dashed lines*, decomposition of spectra into Alq3 (tris-(8-hydroxyquinoline)aluminum) and QD components. *Inset*, cartoon of a QD of the core-shell type. Solutions of QDs have a PL efficiency of $22 \pm 2\%$. Absorption and luminescence spectra of the QD solutions peak at wavelengths of 545 and 561 nm, respectively, corresponding to a CdSe core diameter of ~ 38 Å coated with 1.5 monolayers of ZnS. The QDs are mixed into a chloroform solution of *N*,*N*′-diphenyl-*N*,*N*′-bis(3-methylphenyl)-(1,1′-biphenyl)-4,4′-diamine (TPD), which is then spin-cast onto clean, ITO-coated glass substrates. The QD and TPD concentrations are optimized such that spin-casting results in the formation of a single QD monolayer on top of a 35-nm-thick TPD layer. **a** For device I, a 40 nm-thick film of Alq3 is then thermally evaporated, followed by a 1 mm-diameter, 75 nm-thick Mg : Ag (10 : 1 by mass) cathode with a 50 nm Ag cap. **b** For device II, a layer of 3-(4-biphenyl)-4-phenyl-5-*t*-butylphenyl-1,2,4-triazole (TAZ) with a nominal thickness of 10 nm is evaporated before a 30 nm Alq3 deposition. The spin-casting and device manipulation during growth is performed in a dry nitrogen environment, with moisture and oxygen contents of less than 5 p.p.m. All measurements are done in air. For optimized growth conditions, device yields are high compared to those of thermally evaporated all-organic LEDs. *f*, emission fraction [93]

Bulovic and Bawendi et al. recently reported on the fabrication of high-efficiency organic LEDs in which the light-emitting centers are a single monolayer of CdSe NCs, as shown in Fig. 39 [93]. Previously, poor conduction through NC multilayers led to an injected charge imbalance, and consequently the luminescence efficiency of these early devices never exceeded 0.10 cd/A. A high density of pinhole defects in NC multilayers resulted in low device yields and inconsistent device performance. These technological shortcomings are avoided in structures that use only a single monolayer of QDs as the emissive layer (Fig. 39). The spectral peak 562 nm is attributed to emission from the CdSe NCs. Remarkably, the efficiency of the devices is about 25 times higher than that achieved so far with quantum-dot LEDs.

3.3.4 CdSe/ZnS Core-Shell NC Film

Hikmet et al. studied the charge transport and EL properties of colloidally-synthesized CdSe/ZnS core-shell NC QDs [27]. NCs were prepared via pyrolysis of organometallic reagents in a hot coordinating solvent medium. Thin film diodes were produced by depositing a layer of QDs on top of a layer of the conducting polymer poly(3,4-ethylenedioxythiophene) (PEDOT): polystyrenesulfonate (PSS) and then depositing a metal electrode, as shown in Fig. 40. Only a small rectification could be observed upon reversing the bias for all of the metals used in this study. In Fig. 41, the current and the emitted light intensity are plotted as a function of voltage. Light emission was activated at about 5 V when PEDOT was at a positive bias and at 7 V when it was at a negative bias.

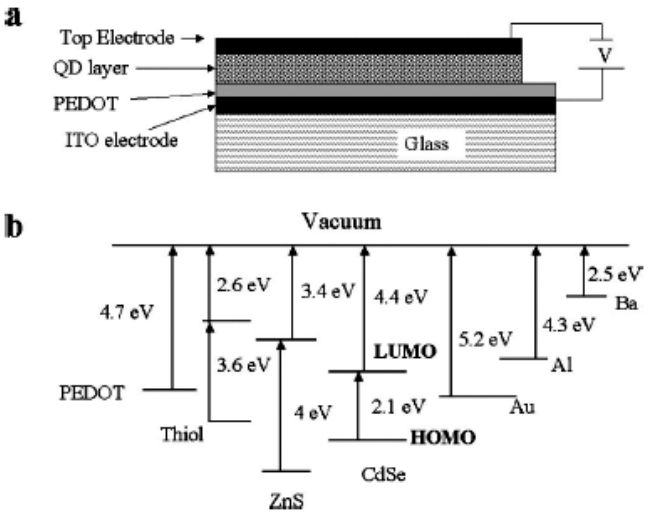

Fig. 40 **a** Structure of the device and **b** energy levels of various materials used [27]

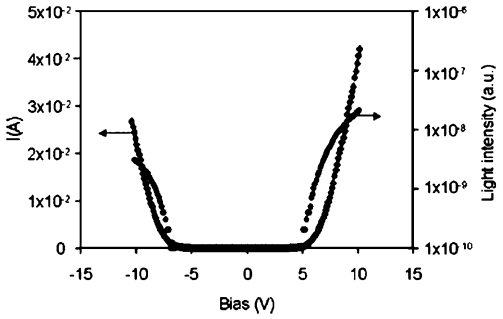

Fig. 41 Current and light intensity as a function of voltage [27]

The efficiency of the light generation showed a strong dependence on the work function and bias of the metal electrodes, and light generation in these devices was proposed to occur by recombination of injected holes and electrons. The difficulty encountered when injecting holes into the QDs was attributed to the low-lying HOMO level of CdSe QDs, and this was considered to be the cause of the low efficiencies observed. The voltage dependence of the current in QD composites could be explained by a space charge-limited current (SCLC) in the presence of defects. At low voltages, the QD layers showed ohmic behavior. At intermediate voltages, the I-V behavior could be described by SCLC with traps. At high voltages the traps became filled and SCLC without traps could be used to describe the voltage dependence of the current. The fact that SCLC could be used to describe the observed behavior supported the suggestion that electrons were the majority carriers in the diodes. The calculated low mobility for the QD layers indicated that a hopping conduction mechanism was used. The trap density was estimated to be roughly the same as the number density of QDs, indicating that each QD acts as an electron trap.

Bawendi et al. [95] also investigated the charge injection quenching of the photoluminescence of ZnS-CdSe core-shell NCs. Experimental results were compared with those of pure CdSe devices. The core-shell NCs were said to have an inefficient charging process and a dynamic competition between charge injection through the ZnS layer and photo-assisted discharging of the core via interface trap states [95].

3.3.5 Electrochemistry and ECL of CdSe, CdSe/CdS Core-Shell NC Film and InP NC Solution

Nann and co-workers recently investigated ionization, electron affinity and quantum confinement in CdSe NCs, using cyclic voltammetry of their film dip-coated onto Au electrodes [96]. The electrochemical results are in total

agreement with the theoretical expectations (quantum confinement) and the spectroscopic data as shown in Table 2.

Very recently, Weller et al. reported the ECL observations from a cross-linked CdSe NC film with 1,8-octanediamine at platinum or F-doped SnO_2

Table 2 Estimated band gap energies for different CdSe NCs by three methods: absorption onset E_g, photoluminescence maximum E_g', and electrochemical determination ΔE [96]

	3.23 nm	3.48 nm	3.73 nm	3.80 nm
E_g (eV)	2.10	2.05	2.01	2.00
E_g' (eV)	2.17	2.13	2.08	2.05
ΔE (V)	2.10	2.03	1.99	1.94

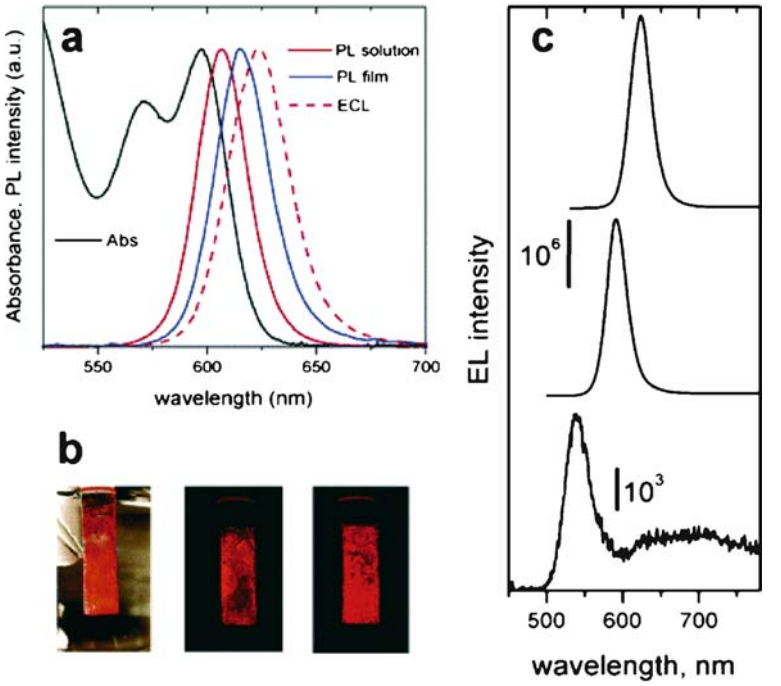

Fig. 42 **a** Absorbance of 5.1 nm CdSe nanocrystals dispersed in chloroform (from *left* to *right*; *left peak*) and PL spectra measured on the same nanocrystals dispersed in chloroform (*second peak* from the *left*) and cross-linked by 1,8-octanediamine into a close-packed film (*third peak* from the *left*). The ECL spectrum of the cross-linked film is shown by *dashed line*. **b** True color photographs of an electrode with a film of 4.3 nm CdSe nanocrystals (*left*), and ECL observed on CdSe nanocrystals with diameters of 4.3 nm (*middle photo*) and 5.1 nm (*right photo*). **c** ECL spectra of the cross-linked films of 2.8, 4.2, and 5.1 nm CdSe nanocrystals

substrates in contact with a peroxodisulfate solution as the co-reactant [97]. Green, yellow and red ECL was emitted from 2.8, 4.2 and 5.1 nm CdSe NCs respectively (Fig. 42). The films of cross-linked CdSe/CdS core-shell NCs exhibited ECL that was about two orders of magnitude weaker than that of CdSe NCs, possibly due to their poor conductivity. It was found that the addition of hydrogen peroxide induces ECL of CdSe/CdS core-shell nanocrystals [97]. ECL can be also generated from a colloidal solution of 4.2 nm InP NCs in butanol upon the addition of hydrogen peroxide [97].

4 Perspective and Conclusions

Electrochemical measurements of NCs have already demonstrated that they can provide useful information about redox potentials, energy levels, band gaps, and particle stability on doping. However, most of the work described here must still be considered preliminary, and more detailed and definitive results are needed. A problem with measurements of NC solutions is the low solubility of the particles (at the μM level) and the low diffusion coefficients of the particles ($\sim 10^{-7}$ cm^2/s), resulting in current levels during CV that are difficult to measure above the background signal. A way to improve the solubility is needed, for example by finding alternative capping ligands and solvents. More work also needs to be carried out with solvents that have larger potential windows and in which compound semiconductor particles are more stable. Higher stability is important, for example, in obtaining higher intensity ECL and when utilizing NCs as ECL labels.

Thin films allow a better electrochemical signal and are more closely related to potential devices. Size-controlled and, therefore, band gap-engineered semiconductor NCs may find use in a wide range of electrical and optical applications. Light emission through EL or ECL in the visible region may find possible applications in displays, optoelectronics and microelectronics.

Acknowledgements The contributions of Bernadette M. Quinn, Santosh K. Haram, Brian A. Korgel, Lindsay E. Pell, Mihai Buda, Gregory Kalyuzhny and Yoonjung Bae are greatly acknowledged. We thank Paul Barbara, F.-R. F. Fan, Rebecca Y. Lai, Zhonghua Yu, Janine Mauzeroll, Ilwhan Oh, and Jai-Pil Choi for their valuable discussions.

Financial support of this project by the National Science Foundation (CHE 0202136) and the Robert A. Welch Foundation is greatly appreciated. ZFD wishes to thank the National Sciences and Engineering Research Council of Canada, the Canada Foundation for Innovation (CFI), the Ontario Innovation Trust (OIT), the Premier's Research Excellence Award (PREA) and the University of Western Ontario (Academic Development Fund (ADF) and a Start-up Fund) for their financial support. He would also thank the Swiss Federal Institute of Technology (EPFL) for a visiting professorship in 2003.

References

1. Hodes G (ed) (2001) Wiley-VCH, Weinheim, p 310
2. O'Regan B, Moser J, Anderson M, Gratzel M (1990) J Phys Chem 94:8720
3. Frank SN, Bard AJ (1977) J Am Chem Soc 99:303
4. Dunn W, Aikawa Y, Bard AJ (1981) J Electrochem Soc 128:222
5. Dunn W, Aikawa Y, Bard AJ (1981) J Am Chem Soc 103:3456
6. Bard AJ, Pruiksma R, White JR, Dunn W, Ward MD (1982) In: Wallace WL, Nozik AJ, Deb SK, Wilson RH (eds) Photoelectrochemistry: Fundamental processes and measurement techniques, Vol 82-3. The Electrochemical Society, Pennington, NJ p 381
7. Ward MD, Bard AJ (1982) J Phys Chem 86:3599
8. Ward MD, White JR, Bard AJ (1983) J Am Chem Soc 105:27
9. White JR, Bard AJ (1985) J Phys Chem 89:1947
10. Serpone N, Borgarello E, Pelizzetti E (1988) J Electrochem Soc 135:2760
11. Chen G, Zen J-M, Fan F-RF, Bard AJ (1991) J Phys Chem 95:3682
12. Albery WJ, Bartlett PN, Porter JD (1984) J Electrochem Soc 131:2896
13. Heyrovsky M, Jirkovsky J (1996) Langmuir 11:4288
14. Ogawa S, Fan F-RF, Bard AJ (1995) J Phys Chem 99:11182
15. Ogawa S, Hu K, Fan F-RF, Bard AJ (1997) J Phys Chem 29:5707
16. Hotchandani S, Bedja I, Richard J, Fessenden W, Kamat PV (1994) Langmuir 10:17
17. Fabregat-Santiago F, Mora-Sero I, Garcia-Belmonte G, Bisquert J (2003) J Phys Chem B 107:758
18. Holmes JD, Ziegler KJ, Doty RC, Pell LE, Johnston KP, Korgel BA (2001) J Am Chem Soc 123:3743
19. Ziegler KJ (2001) PhD Dissertation. University of Texas, Austin, TX
20. Murray CB, Norris DJ, Bawendi MG (1993) J Am Chem Soc 115:8706
21. Chemseddine A, Weller H (1993) Ber Bunsen-Ges 97:636
22. Vossmeyer T, Katsikas L, Giersig M, Popovic IG, Diesner K, Chemseddine A, Eychmueller A, Weller H (1994) J Phys Chem 98:7665
23. Peng ZA, Peng X (2001) J Am Chem Soc 123:183
24. Qu L, Peng ZA, Peng X (2001) Nano Lett 1:333
25. Peng X (2002) Chem Eur J 8:334
26. Chen S, Truax LA, Sommers JM (2000) Chem Mater 12:3864
27. Hikmet RAM, Talapin DV, Weller H (2003) J Appl Phys 93:3509
28. Wehrenberg BL, Wang C, Guyot-Sionnest P (2002) J Phys Chem B 106:10634
29. Talapin DV, Rogach AL, Kornowski A, Haase M, Weller H (2001) Nano Lett 1:207
30. Murray CB, Kagan CR, Bawendi MG (2000) Annu Rev Mater Sci 30:545
31. Girault HH (2001) Electrochimie physique et analytique. PPUR, Lausanne
32. Bard AJ, Faulkner LR (2001) Electrochemical methods, fundamentals and applications. Wiley, New York
33. Franceschetti A, Zunger A (2000) Phys Rev B 62:2614
34. Chen S, Ingrma RS, Hostetler MJ, Pietron JJ, Murray RW, Schaaff TG, Khoury JT, Alvarez MM, Whetten RL (1998) Science 280:2098
35. Hanna AE, Tuominen MT, Tinkham M (1992) Phys Rev Lett 68:3228
36. Fan F-RF, Bard AJ (1997) Science 277:1791
37. Andres RP, Bein T, Dorogi M, Feng S, Henderson JI, Kubiak CP, Mahoney W, Osifchin RG, Reifenberger R (1996) Science 272:1323
38. Murphy CJ (2002) Anal Chem 74:520A
39. Quinn BM, Liljeroth P, Ruiz V, Laaksonen T, Kontturi K (2003) J Am Chem Soc 125:6644

40. Banin U, Cao Y, Katz D, Millo O (1999) Nature 400:542
41. Sokol WF, Evans DH (1981) Anal Chem 53:578
42. Faulkner LR, Bard AJ (1977) In: Bard AJ (ed) Electroanalytical chemistry, Vol 10. Dekker, New York, p 1
43. Knight AW, Greenway GM (1994) Analyst 119:879
44. Ding Z, Buda M, Pell LE, Korgel BA, Bard AJ (unpublished results)
45. Kalyuzhny G, Buda M, McNeill J, Barbara P, Bard AJ (2003) J Am Chem Soc 125:6272
46. Gao FG, Bard AJ (2002) Chem Mater 14:3465
47. English DS, Pell LE, Yu Z, Barbara PF, Korgel BA (2002) Nano Lett 2:681
48. Lin C-W, Lin S-Y, Lee S-C, Chia C-T (2002) J Appl Phys 91:1525
49. Wu Y, Yang P (2001) Adv Mater 13:520
50. Wilcoxon JP, Provencio PP, Samara GA (2001) Phys Rev B 64:035417/1
51. Niquet YM, Allan G, Delerue C, Lannoo M (2000) Appl Phys Lett 77:1182
52. Ding Z, Quinn BM, Haram SK, Pell LE, Korgel BA, Bard AJ (2002) Science 296:1293
53. Chen S, Murray RW, Feldberg SW (1998) J Phys Chem B 102:9898
54. Haram SK, Quinn BM, Bard AJ (2001) J Am Chem Soc 123:8860
55. Puzder A, Williamson AJ, Grossman JC, Galli G (2002) Phys Rev Lett 88:097401/1
56. Wilcoxon JP, Samara GA, Provencio PN (1999) Phys Rev B 60:2704
57. Nirmal M, Brus L (1999) Acc Chem Res 32:407
58. Kovalev D, Heckler H, Ben-Chorin M, Polisski G, Schwartzkopff M, Koch F (1998) Phys Rev Lett 81:2803
59. Iyer SS, Xie YH (1993) Science 260:40
60. Holmes JD, Johnston KP, Doty RC, Korgel BA (2000) Science 287:1471
61. McCord P, Yau SL, Bard AJ (1992) Science 257:68
62. Shim M, Guyot-Sionnest P (2000) Nature 407:981
63. Wang C, Shim M, Guyot-Sionnest P (2001) Science 291:2390
64. Makimura T, Kunii Y, Ono N, Murakami K (1998) Appl Surf Sci 127–129:388
65. Choi HC, Buriak JM (2000) Chem Mater 12:2151
66. Myung N, Lu X, Johnston KP, Bard AJ (2004) Nano Lett 4:183
67. Myung N, Ding Z, Bard AJ (2002) Nano Lett 2:1315
68. Ren T, Xu J-Z, Tu Y-F, Xu S, Zhu J-J (2005) Electrochem Comm 7:5
69. Guyot-Sionnest P, Wang C (2003) J Phys Chem 107:7355
70. Hines MA, Guyot-Sionnest P (1996) J Phys Chem 100:468
71. Danek M, Jensen KF, Murray CB, Bawendi MG (1996) Chem Mater 8:173
72. Zhou J, Zhu J, Brzezinski J, Ding Z (submitted) J Phys Chem B
73. Alperson B, Rubinstein I, Hodes G, Porath D, Millo O (1999) Appl Phys Lett 75:1751
74. Bae Y, Myung N, Bard AJ (2004) Nano Lett 4:1153
75. Zhou J, Zhu J, Ding Z (2005) In: Chang PC, Shiojima K, Kopf RE, Buckley DN, Etcheberry A, Marsen B (eds) 207th Meeting of the ECS, Vol 2005-04, The ECS, Quebec City, p 129
76. Wu XC, Bittner AM, Kern K (2005) J Phys Chem B 109:230
77. Myung N, Bae Y, Bard AJ (2003) Nano Lett 3:1053
78. Reiss P, Bleuse J, Pron A (2002) Nano Lett 2:781
79. Bruchez M, Moronne M, Gin P, Weiss S, Alivisatos APS (1998) Science 281:2013
80. Schlamp MC, Peng X, Alivisatos AP (1997) J Appl Phys 82:5837
81. Peng X, Schlamp MC, Kadavanich AV, Alivisatos AP (1997) J Am Chem Soc 119:7019
82. Gao M, Sun J, Dulkeith E, Gaponik N, Lemmer U, Feldmann J (2002) Langmuir 18:4098
83. Greene IA, Wu F, Zhang JZ, Chen S (2003) J Phys Chem B 107:5733
84. Ushida K, Yoshida Y, Kozawa T, Tagawa S, Kira A (1999) J Phys Chem A 103:4680

85. Nicol MJ, Paul RL, Diggle JW (1978) Electrochim Acta 23:635
86. Paul RL, Nicol MJ, Diggle JW, Saunders AP (1978) Electrochim Acta 23:625
87. Gao FG, Bard AJ (2000) J Am Chem Soc 122:7426
88. Buda M, Kalyuzhny G, Bard AJ (2002) J Am Chem Soc 124:6090
89. Nishimura K, Nagao Y (2000) J Porous Mater 7:119
90. Gudiksen MS, Lauhon UJ, Wang J, Smith DC, Lieber CM (2002) Nature 415:617
91. Haneman D, Yuan J (1997) Appl Surf Sci 113:103
92. Wehrenberg BL, Guyot-Sionnest P (2003) J Am Chem Soc 125:7806
93. Coe S, Woo W-K, Bawendi M, Bulovic V (2002) Nature 420:800
94. Wang C, Shim M, Guyot-Sionnest P (2002) Appl Phys Lett 80:4
95. Woo W-K, Shimizu KT, Jarosz MV, Neuhauser RG, Leatherdale CA, Rubner MA, Bawendi MG (2002) Adv Mater 14:1068
96. Kucur E, Riegler J, Urban GA, Nann T (2003) J Chem Phys 119:2333
97. Poznyak SK, Talapin DV, Shevchenko EV, Weller H (2004) Nano Lett 4:693